Scrutinizing the Alignment Limit in Two-Higgs-Doublet Models

Part 2: $m_H = 125$ GeV

Jérémy Bernon[1][*], John F. Gunion[2][†], Howard E. Haber[3][‡], Yun Jiang[2,4][§], Sabine Kraml[1][¶]

[1] *Laboratoire de Physique Subatomique et de Cosmologie, Université Grenoble-Alpes, CNRS/IN2P3, 53 Avenue des Martyrs, F-38026 Grenoble, France*

[2] *Department of Physics, University of California, Davis, CA 95616, USA*

[3] *Santa Cruz Institute for Particle Physics, Santa Cruz, CA 95064, USA*

[4] *NBIA and Discovery Center, Niels Bohr Institute, University of Copenhagen, Blegdamsvej 17, DK-2100, Copenhagen, Denmark*

Abstract

In the alignment limit of a multi-doublet Higgs sector, one of the Higgs mass eigenstates aligns in field space with the direction of the scalar field vacuum expectation values, and its couplings approach those of the Standard Model (SM) Higgs boson. We consider CP-conserving Two-Higgs-Doublet Models (2HDMs) of Type I and Type II near the alignment limit in which the heavier of the two CP-even Higgs bosons, H, is the SM-like state observed with a mass of 125 GeV, and the couplings of H to gauge bosons approach those of the SM. We review the theoretical structure and analyze the phenomenological implications of this particular realization of the alignment limit, where decoupling of the extra states cannot occur given that the lighter CP-even state h must, by definition, have a mass below 125 GeV. For the numerical analysis, we perform scans of the 2HDM parameter space employing the software packages 2HDMC and Lilith, taking into account all relevant pre-LHC constraints, constraints from the measurements of the 125 GeV Higgs signal at the LHC, as well as the most recent limits coming from searches for other Higgs-like states. Implications for Run 2 at the LHC, including expectations for observing the other scalar states, are also discussed.

[*]Email: bernon@lpsc.in2p3.fr

[†]Email: jfgunion@ucdavis.edu

[‡]Email: haber@scipp.ucsc.edu

[§]Email: yunjiang@nbi.ku.dk

[¶]Email: sabine.kraml@lpsc.in2p3.fr

arXiv:1511.03682v2 [hep-ph] 29 Nov 2015

1 Introduction

While the Higgs boson measurements at Run 1 of the LHC [1–3] (see also [4, 5]) show no deviations from Standard Model (SM) expectations, conceptually there is no reason why the Higgs sector should be minimal. Indeed a non-minimal Higgs sector is theoretically very attractive and, if confirmed, would shine a new light on the dynamics of electroweak symmetry breaking. The challenge for Run 2 of the LHC, and other future collider programs, is to determine whether the observed state with mass 125 GeV is *the* SM Higgs boson, or whether it is part of a non-minimal Higgs sector of a more fundamental theory.

In models with a multi-doublet Higgs sector such as the Two-Higgs-Doublet Model [6, 7] (2HDM), which is the focus of our study, a special situation arises when one of the Higgs mass eigenstates is approximately aligned in field space with the direction of the scalar field vacuum expectation values (vevs). This motivates the introduction of the Higgs basis, in which the scalar vev resides entirely in one linear combination of scalar fields. In the approach to the so-called *alignment limit*,[1] the $W^\pm$ and Z gauge bosons dominantly acquire their masses from the Higgs doublet of the Higgs basis with the non-zero vev, and the coupling of that Higgs boson to W^+W^- (and ZZ) tends toward its SM value, $C_V \to 1$.[2] Of course, for consistency with the LHC measurements, this Higgs boson must then be identified with the observed SM-like state at 125 GeV.

In a recent paper [15], we provided a comprehensive study of the alignment limit in the context of CP-conserving 2HDMs of Type I and Type II, assuming that the observed 125 GeV state is the lighter of the two CP-even Higgs bosons, h, in these models. Whereas alignment is automatically attained in the decoupling limit in the case of $m_h = 125$ GeV when the additional Higgs states H, A, $H^\pm$ are very heavy, it can also occur when the additional Higgs states are light, i.e. alignment without decoupling [8]. The purpose of [15] was to investigate the phenomenological consequences of alignment without decoupling in the $m_h = 125$ GeV scenario and contrast the resulting phenomenology to the case of decoupling. In this paper, we now focus on the equally interesting but much less studied possibility that the observed 125 GeV state is the heavier H of the two CP-even Higgs bosons of the 2HDM. In this case, alignment is always attained without decoupling, since by definition h is lighter than H. Furthermore, the masses of the CP-odd Higgs boson A and the charged Higgs boson $H^\pm$ are limited by the requirements of stability, perturbativity and electroweak precision measurements. The alignment limit in the $m_H = 125$ GeV scenario therefore offers a very specific phenomenology that is worth contrasting to that of the $m_h = 125$ GeV scenario.

The paper is organized as follows. In Section 2 we elaborate on theoretical considerations that are specific to the alignment limit in the case of $m_H = 125$ GeV. The numerical results of our study are presented in Section 3. Two aspects are considered in detail: the precision measurements of the couplings and signal strengths of the SM-like Higgs boson at 125 GeV, and the ways to discover the additional Higgs states of the 2HDM when they are light. Section 4 presents our conclusions. Throughout the paper we follow the notation and conventions used in [15]. The setup of the numerical analysis and the constraints applied also follow [15]. In

---

[1]Aspects of the alignment limit were first emphasized in [8] and investigated further in [9–14].

[2]We use the notation of coupling scale factors, or *reduced couplings*, employed in [4]: C_V ($V = W, Z$) for the coupling to gauge bosons, $C_{U,D}$ for the couplings to up-type and down-type fermions and $C_{\gamma,g}$ for the loop-induced couplings to photons and gluons.

addition, we consider the new CMS limit [16] for light neutral Higgs bosons with masses between 25 GeV and 80 GeV, produced in association with a pair of b quarks and decaying into $\tau\tau$. Moreover, we take into account the CMS limits [17] on $gg \to A \to Zh$ with $Z \to \ell\ell$ and $h \to b\bar{b}$ or $\tau\tau$, which significantly constrain the scenario studied in this paper (but are much less relevant for the analysis of [15]). Details on the CMS $gg \to A \to Zh$ limits and their impact on the 2HDM parameter space are given in the Appendix.

2 Theoretical considerations

In this section, we expand on the theoretical discussion in [15] (see also [18]), treating questions that are relevant specifically for a SM-like H at 125 GeV. It is convenient to work in the Higgs basis [19, 20], where the vev, $v = 2m_W/g \simeq 246$ GeV, resides entirely in one of the two Higgs doublet fields,

$$\langle H_1^0 \rangle = v/\sqrt{2} \quad \text{and} \quad \langle H_2^0 \rangle = 0 \,. \tag{1}$$

The scalar potential in the Higgs basis is

$$\mathcal{V} = Y_1 H_1^\dagger H_1 + Y_2 H_2^\dagger H_2 + Y_3 [H_1^\dagger H_2 + \text{h.c.}] + \tfrac{1}{2} Z_1 (H_1^\dagger H_1)^2 + \tfrac{1}{2} Z_2 (H_2^\dagger H_2)^2 + Z_3 (H_1^\dagger H_1)(H_2^\dagger H_2)$$

$$+ Z_4 (H_1^\dagger H_2)(H_2^\dagger H_1) + \left\{ \tfrac{1}{2} Z_5 (H_1^\dagger H_2)^2 + \left[Z_6 (H_1^\dagger H_1) + Z_7 (H_2^\dagger H_2) \right] H_1^\dagger H_2 + \text{h.c.} \right\}, \tag{2}$$

where $Y_1 = -\tfrac{1}{2} Z_1 v^2$ and $Y_3 = -\tfrac{1}{2} Z_6 v^2$ at the scalar potential minimum. For simplicity, we assume that the field H_2 can be rephased such that the potentially complex parameters Z_5, Z_6 and Z_7 are real, in which case the scalar potential and Higgs vacuum are CP-conserving. Henceforth, we will always adopt such a "real basis".[3] In order to preserve perturbativity and tree-level unitarity [21–26], the dimensionless couplings Z_i cannot be taken arbitrary large. Generically, the Z_i are $\mathcal{O}(1)$ constants, although it is possible for some of the Z_i to be as large as ~ 10 without violating any low-energy constraints.[4]

Under the assumption of a CP-conserving Higgs sector, the Higgs mass spectrum is easily determined. The squared-masses of the charged Higgs and CP-odd Higgs bosons are given by

$$m_{H^\pm}^2 = Y_2 + \tfrac{1}{2} Z_3 v^2 \,, \tag{3}$$

$$m_A^2 = m_{H^\pm}^2 + \tfrac{1}{2}(Z_4 - Z_5)v^2 \,, \tag{4}$$

and the two CP-even squared masses are obtained by diagonalizing the CP-even Higgs squared-mass matrix,

$$\mathcal{M}_H^2 = \begin{pmatrix} Z_1 v^2 & Z_6 v^2 \\ Z_6 v^2 & m_A^2 + Z_5 v^2 \end{pmatrix} . \tag{5}$$

The physical mass eigenstates are

$$H = (\sqrt{2} \,\text{Re}\, H_1^0 - v) c_{\beta-\alpha} - \sqrt{2} \,\text{Re}\, H_2^0 \, s_{\beta-\alpha} \,, \tag{6}$$

$$h = (\sqrt{2} \,\text{Re}\, H_1^0 - v) \, s_{\beta-\alpha} + \sqrt{2} \,\text{Re}\, H_2^0 \, c_{\beta-\alpha} \,, \tag{7}$$

---

[3]No rephasing of H_1 is permitted since by assumption the vev v is real and positive.

[4]Taking the Z_i significantly larger than $\mathcal{O}(1)$ will lead to Landau poles at an energy scale below the Planck scale [27–30]. However, we shall take an agnostic view in our scans by treating the 2HDM as an effective low-energy theory with no assumptions on its behavior at higher energies.

where $m_h \leq m_H$. In Eqs. (6) and (7), the CP-even Higgs mixing angle in the Higgs basis is denoted by $\alpha - \beta$ and the notation $c_{\beta-\alpha} \equiv \cos(\beta - \alpha)$ and $s_{\beta-\alpha} \equiv \sin(\beta - \alpha)$ is employed. The resulting CP-even Higgs squared-masses are given by

$$m_{H,h}^2 = \tfrac{1}{2}\left[m_A^2 + (Z_5 + Z_1)v^2 \pm \sqrt{[m_A^2 + (Z_5 - Z_1)v^2]^2 + 4Z_6^2 v^4}\right]. \tag{8}$$

In light of Eq. (1), if $\sqrt{2}\,\mathrm{Re}\,H_1^0 - v$ were a mass eigenstate, then its tree-level couplings to SM particles and its self-couplings would be precisely those of the SM Higgs boson. That is, if one of the neutral CP-even Higgs mass eigenstates is approximately aligned in field space with the direction of the vev (the so-called alignment limit), then the couplings of this Higgs boson are SM-like. In [15], we examined the case of a SM-like h, where alignment can be achieved in two ways. First, in the decoupling limit of the 2HDM with $m_A \gg v$, the mixing of states in Eq. (5) is automatically negligible. Second, alignment without decoupling occurs if $|Z_6|v^2 \ll Z_1 v^2 < m_A^2 + Z_5 v^2$. In both cases, $h \simeq \sqrt{2}\,\mathrm{Re}\,H_1^0 - v$, corresponding to $|c_{\beta-\alpha}| \ll 1$.

In this paper we consider the case in which the heavier of the two CP-even neutral scalars H is identified as the SM-like Higgs boson with a mass of 125 GeV. Equations (6) and (7) then imply that $H \simeq \sqrt{2}\,\mathrm{Re}\,H_1^0 - v$, corresponding to $|s_{\beta-\alpha}| \ll 1$. A SM-like H can only be achieved if

$$m_A^2 + Z_5 v^2 < Z_1 v^2\,, \tag{9}$$

$$|Z_6|v^2 \ll |m_A^2 + (Z_5 - Z_1)v^2|\,, \tag{10}$$

in which case the CP-even Higgs squared masses are given by

$$m_H^2 = Z_1 v^2 + \frac{Z_6^2 v^4}{|m_A^2 + (Z_5 - Z_1)v^2|} + \mathcal{O}(Z_6^4)\,, \tag{11}$$

$$m_h^2 = m_A^2 + Z_5 v^2 - \frac{Z_6^2 v^4}{|m_A^2 + (Z_5 - Z_1)v^2|} + \mathcal{O}(Z_6^4)\,, \tag{12}$$

in the approach to the alignment limit. In contrast to the case of a SM-like h, there is no analog of the decoupling limit in which H is SM-like since h is necessarily lighter than H, and the masses of $H^\pm$ and A are typically of $\mathcal{O}(v)$ in light of Eqs. (4) and (9).

The physical masses of the neutral scalars are related by the following exact expressions,

$$Z_1 v^2 = m_h^2 s_{\beta-\alpha}^2 + m_H^2 c_{\beta-\alpha}^2\,, \tag{13}$$

$$Z_6 v^2 = (m_h^2 - m_H^2)s_{\beta-\alpha}c_{\beta-\alpha}\,, \tag{14}$$

$$Z_5 v^2 = m_H^2 s_{\beta-\alpha}^2 + m_h^2 c_{\beta-\alpha}^2 - m_A^2\,. \tag{15}$$

Using Eqs. (4) and (15), it also follows that

$$Z_4 v^2 = m_H^2 s_{\beta-\alpha}^2 + m_h^2 c_{\beta-\alpha}^2 + m_A^2 - 2m_{H^\pm}^2\,. \tag{16}$$

These equations exhibit all the features discussed above. In the exact alignment limit where H is identified as the SM Higgs boson and $s_{\beta-\alpha} = 0$, we see that $Z_6 = 0$, $m_h^2 = m_A^2 + Z_5 v^2$, $m_H^2 = Z_1 v^2$ and the inequalities of Eqs. (9) and (10) are satisfied. Indeed, all Higgs boson

3

masses are of $\mathcal{O}(v)$ in this limit. In contrast, if $Z_6 = 0$ is satisfied by taking $c_{\beta-\alpha} = 0$, it is evident that it is h that is SM-like.

The consequences of Eqs. (13)–(15) obtained in [15] were written in a form that was convenient for the case in which h is the SM-like Higgs boson, i.e. where $|c_{\beta-\alpha}| \ll 1$. In the case where H is the SM-like Higgs boson, i.e. $|s_{\beta-\alpha}| \ll 1$, it is more useful rewrite the expressions obtained from Eqs. (13)–(15) as follows,

$$m_H^2 = \left(Z_1 - Z_6 \frac{s_{\beta-\alpha}}{c_{\beta-\alpha}} \right) v^2 \,, \tag{17}$$

$$m_h^2 = m_A^2 + \left(Z_5 + Z_6 \frac{s_{\beta-\alpha}}{c_{\beta-\alpha}} \right) v^2 \,. \tag{18}$$

Note that Eqs. (13) and (14) imply that

$$Z_6 s_{\beta-\alpha} c_{\beta-\alpha} \leq 0 \,, \tag{19}$$

$$|Z_6| v^2 = \sqrt{(m_H^2 - Z_1 v^2)(Z_1 v^2 - m_h^2)} \,. \tag{20}$$

One can also derive expressions for $c_{\beta-\alpha}$ and $s_{\beta-\alpha}$ directly from Eqs. (13) and (14). In light of Eq. (19), the sign of the product $s_{\beta-\alpha} c_{\beta-\alpha}$ is fixed by the sign of Z_6. However, since $\beta - \alpha$ is defined only modulo π, we are free to choose a convention where either $c_{\beta-\alpha}$ or $s_{\beta-\alpha}$ is always non-negative. A convenient choice of convention is dictated by the form of the couplings of the neutral CP-even Higgs bosons to VV (where $VV = W^+ W^-$ or ZZ). Denoting the ϕVV couplings ($\phi = h, H$) normalized to the corresponding coupling of VV to the SM Higgs boson by C_V^ϕ, it follows that [6,7]

$$C_V^h = s_{\beta-\alpha} \,, \qquad C_V^H = c_{\beta-\alpha} \,, \tag{21}$$

as shown in Table 1.

Since $|s_{\beta-\alpha}| \ll 1$ for a SM-like H, the value of $|c_{\beta-\alpha}|$ must be close to 1. In order to be consistent with the standard presentation of the SM Higgs Lagrangian, we shall choose a convention where $c_{\beta-\alpha}$ is non-negative (so that $C_V^H \to +1$ in the alignment limit). In this convention,

$$s_{\beta-\alpha} = -\operatorname{sgn}(Z_6) \sqrt{\frac{m_H^2 - Z_1 v^2}{m_H^2 - m_h^2}} = \frac{-Z_6 v^2}{\sqrt{(m_H^2 - m_h^2)(Z_1 v^2 - m_h^2)}} \,. \tag{22}$$

In the approach to the alignment limit, we may use Eqs. (11) and (12) to write

$$s_{\beta-\alpha} = \frac{-Z_6 v^2}{|m_A^2 + (Z_5 - Z_1)v^2|} + \mathcal{O}(Z_6^4) \,, \tag{23}$$

subject to the inequality given in Eq. (10).

Having adopted the real Higgs basis in which all the potentially complex parameters of the scalar potential are real, one can still perform a field redefinition $H_2 \to -H_2$, which would flip the signs of Y_3, Z_6 and Z_7. Such a field redefinition has no physical consequence in the most general CP-conserving 2HDM. In particular, the sign of Z_6 is unphysical. Indeed, as previously noted below Eq. (20), only the sign of the product $Z_6 c_{\beta-\alpha} s_{\beta-\alpha}$ is meaningful.

We have emphasized above that if H is SM-like, then we expect all Higgs boson masses to be of $\mathcal{O}(v)$. Nevertheless, a parameter regime exists in which A and/or $H^\pm$ can be considerably heavier than H. To see how this can arise, we rewrite Eqs. (15) and (16) as follows,

$$m_A^2 = m_H^2 s_{\beta-\alpha}^2 + m_h^2 c_{\beta-\alpha}^2 - Z_5 v^2 \,, \tag{24}$$

$$m_{H^\pm}^2 = m_H^2 s_{\beta-\alpha}^2 + m_h^2 c_{\beta-\alpha}^2 - \tfrac{1}{2}(Z_4 + Z_5) v^2 \,. \tag{25}$$

Consequently,

$$m_A \gg m_H \,, m_{H^\pm} \,, \quad \text{if } Z_5 \text{ is large and negative and } |Z_4 + Z_5| \lesssim \mathcal{O}(1) \,, \tag{26}$$

$$m_{H^\pm} \gg m_H \,, m_A \,, \quad \text{if } Z_4 + Z_5 \text{ is large and negative and } |Z_5| \lesssim \mathcal{O}(1) \,, \tag{27}$$

$$m_A \,, m_{H^\pm} \gg m_H \,, \quad \text{if } Z_5 \text{ is large and negative and } |Z_4| \lesssim \mathcal{O}(1) \,, \tag{28}$$

under the condition that the magnitudes of Z_4 and Z_5 are consistent with tree-level unitarity bounds and that the inequality given in Eq. (9) is satisfied. However, none of these three cases above corresponds to a decoupling limit, since in each case the low-energy effective Higgs theory contains at least one additional scalar state (namely h) beyond the SM-like Higgs boson. Note that in the parameter regime where Eqs. (26) or (27) is satisfied, a second scalar state beyond h may be present whose mass lies below $m_H = 125$ GeV. If the conditions of Eq. (26) are satisfied, then $m_{H^\pm} < m_H$ if $(Z_4 + Z_5)v^2 > -2(m_H^2 - m_h^2)c_{\beta-\alpha}^2$ [cf. Eq. (25)]. Similarly, if the conditions of Eq. (27) are satisfied, then $m_A < m_H$ if $Z_5 v^2 > -(m_H^2 - m_h^2)c_{\beta-\alpha}^2$ [cf. Eq. (24)].

So far, the above discussion is applicable to the scalar sector of the most general CP-conserving 2HDM. If we now add the most general Higgs-fermion Yukawa couplings, we encounter tree-level Higgs-mediated flavor-changing neutral currents (FCNCs) that are too large and thus in conflict with experimental data [31,32]. It is well known that these FCNCs can be eliminated by introducing a new basis of scalar fields $\{\Phi_1, \Phi_2\}$, and a $\mathbb{Z}_2$ discrete symmetry, $\Phi_1 \to +\Phi_1$ and $\Phi_2 \to -\Phi_2$ under which the dimension-four terms of the Higgs scalar potential are invariant. This new basis of scalar fields (in which the $\mathbb{Z}_2$ symmetry is manifest) is designated as the $\mathbb{Z}_2$-basis, and is given in terms of the Higgs basis fields by[5]

$$\Phi_1 \equiv H_1 c_\beta - H_2 s_\beta \,, \qquad \Phi_2 \equiv s_\beta H_1 + c_\beta H_2 \,, \tag{29}$$

where

$$c_\beta \equiv \cos\beta = v_1/v \,, \qquad s_\beta \equiv \sin\beta = v_2/v \,, \tag{30}$$

and $\langle \Phi_i^0 \rangle = v_i$ $(i = 1, 2)$. The $\mathbb{Z}_2$ symmetry is then extended to the Higgs-fermion Yukawa couplings such that two of the four Higgs-quark Yukawa interaction terms (and their hermitian conjugates) vanish (and similarly for the Higgs couplings to leptons). There are a number of ways to accomplish this [33,34]. The Type I model is defined by taking all right-handed fermion fields to be odd under the $\mathbb{Z}_2$ symmetry in the Higgs-fermion interactions, whereas in Type II Higgs-fermion interactions, only the up-type right-handed fermion field is odd under the $\mathbb{Z}_2$ symmetry [35].[6] The $\mathbb{Z}_2$ symmetry guarantees that the neutral Higgs-fermion couplings are

---

[5]The translation between the Higgs and $\mathbb{Z}_2$-bases is discussed in detail in [8,15,18,20].

[6]All left-handed fermion fields are even under the $\mathbb{Z}_2$ symmetry in both Type I and Type II models. Note that the down-type quark and charged lepton fields transform in the same way under the $\mathbb{Z}_2$. In principle, two more models can be constructed in which the Higgs–quark Yukawa couplings are of Type I and the Higgs–lepton Yukawa couplings are of Type II, or vice versa [36–40]. We do not consider these model types in this paper.

Table 1: Tree-level vector boson couplings C_V ($V = W, Z$) and fermionic couplings C_U and C_D normalized to their SM values for the two CP-even scalars h, H and the CP-odd scalar A in Type I and Type II 2HDMs [35].

Higgs	Types I and II VV	Type I up quarks	Type I down quarks and leptons	Type II up quarks	Type II down quarks and leptons
h	$\sin(\beta - \alpha)$	$\cos\alpha/\sin\beta$	$\cos\alpha/\sin\beta$	$\cos\alpha/\sin\beta$	$-\sin\alpha/\cos\beta$
H	$\cos(\beta - \alpha)$	$\sin\alpha/\sin\beta$	$\sin\alpha/\sin\beta$	$\sin\alpha/\sin\beta$	$\cos\alpha/\cos\beta$
A	0	$\cot\beta$	$-\cot\beta$	$\cot\beta$	$\tan\beta$

diagonal in flavor space when expressed in the fermion mass-eigenstate basis. The tree-level Type I and Type II couplings of the neutral Higgs bosons to the fermions, normalized to the corresponding couplings of the SM Higgs boson, are given in Table 1.

In particular, note that the normalized couplings of the SM-like H,

$$\frac{\sin\alpha}{\sin\beta} = c_{\beta-\alpha} - s_{\beta-\alpha}\cot\beta\,, \tag{31}$$

$$\frac{\cos\alpha}{\cos\beta} = c_{\beta-\alpha} + s_{\beta-\alpha}\tan\beta\,, \tag{32}$$

approach unity in the limit of $s_{\beta-\alpha} \to 0$ in the convention where $c_{\beta-\alpha}$ is non-negative. That is, in Type I models for small $|s_{\beta-\alpha}|$, we have $C_U^H = C_D^H \equiv C_F^H \simeq C_V^H \simeq 1$ unless $\tan\beta$ is very small (which is excluded by constraints related to stability, unitarity and perturbativity, in particular the requirement of perturbativity of the top Yukawa coupling). Thus, $C_F^H \to 1$ in the alignment limit. In Type II models we arrive at a similar conclusion for the up-type fermion–Higgs Yukawa coupling, namely $C_U^H \to 1$ in the alignment limit. However, $C_D^H \simeq 1$ only when $|s_{\beta-\alpha}\tan\beta| \ll 1$, which means that if $\tan\beta \gg 1$ then the approach to the alignment limit, $C_D^H \to 1$, is delayed.

In the $\mathbb{Z}_2$-basis of scalar fields defined in Eq. (29), α is the CP-even Higgs mixing angle, which is defined modulo π, and $\tan\beta = v_2/v_1$ is the ratio of neutral Higgs vevs [cf. Eq. (30)]. In a convention in which $c_{\beta-\alpha}$ is non-negative, the sign of $s_{\beta-\alpha}$ is determined by Eq. (19). However, in introducing the $\mathbb{Z}_2$-basis, there is freedom to impose an additional sign convention such that the vevs v_1 and v_2 are non-negative. That is, we assume henceforth that $\tan\beta$ is non-negative, or equivalently,

$$0 \le \beta \le \tfrac{1}{2}\pi\,. \tag{33}$$

For non-negative $\tan\beta$ and $c_{\beta-\alpha}$, it is clear from Eqs. (31) and (32) that the sign of $s_{\beta-\alpha}$ is physically relevant. In light of Eq. (22), it also follows that the sign of Z_6 is now meaningful. These observations can be understood in another way as follows. Since $\tan\beta$ is assumed to be non-negative, one is no longer permitted to perform field redefinitions that change the relative sign of Φ_1 and Φ_2. Using Eq. (29), it then follows that one is no longer permitted to perform a redefinition of the Higgs basis field $H_2 \to -H_2$. But, we previously used such a field redefinition to conclude that the signs of Z_6 and $s_{\beta-\alpha}$ are unphysical [see the text following Eq. (23)]. This is no longer possible once we fix a convention where $\tan\beta$ is non-negative.

6

Another common choice in the literature is to take $-\frac{1}{2}\pi \leq \alpha \leq \frac{1}{2}\pi$ along with Eq. (33), in which case parameter regimes exist in which $c_{\beta-\alpha}$ and/or $s_{\beta-\alpha}$ can take on either sign. It is a simple matter to translate among the various conventions. For example, given any 2HDM parameter point (α, β) with $-\frac{1}{2}\pi \leq \alpha \leq \frac{1}{2}\pi$ and $0 \leq \beta \leq \frac{1}{2}\pi$, one can compute the values of $s_{\beta-\alpha}$ and $c_{\beta-\alpha}$. Then, to convert to the convention of non-negative $c_{\beta-\alpha}$, one would simply replace

$$(s_{\beta-\alpha}, c_{\beta-\alpha}) \to (-s_{\beta-\alpha}, -c_{\beta-\alpha}) \tag{34}$$

if $c_{\beta-\alpha}$ is initially negative. Only the *relative* sign of $s_{\beta-\alpha}$ and $c_{\beta-\alpha}$ is physical for a given sign choice of Z_6 in light of Eq. (19).

Let us now examine the number of parameters that govern the CP-conserving 2HDM of Types I and II. In order to ensure the absence of tree-level Higgs-mediated FCNCs, it is sufficient to impose the $\mathbb{Z}_2$ discrete symmetry introduced above on all dimension-four terms of the Higgs Lagrangian. Thus, we are free to include terms in the Higgs Lagrangian that softly break the symmetry. There exists precisely one term of this type, namely the following dimension-two term that can be added to the scalar potential in the $\mathbb{Z}_2$-basis,

$$V_{\rm soft} = -m_{12}^2 \Phi_1^\dagger \Phi_2 + {\rm h.c.} \tag{35}$$

The squared-mass parameter m_{12}^2 is related to the Higgs basis parameters and the angle β via

$$m_{12}^2 = \tfrac{1}{2}\left(Y_2 + \tfrac{1}{2}Z_1 v^2\right)\sin 2\beta + \tfrac{1}{2}Z_6 v^2 \cos 2\beta \,. \tag{36}$$

Note that if $\sin 2\beta = 0$, then the $\mathbb{Z}_2$ basis and the Higgs basis coincide[7] (cf. Eqs. (24) and (25) of [15]) and $Z_6 = Z_7 = 0$. The latter implies that $m_{12}^2 = 0$ in light of Eq. (36). That is, if $\beta = 0$ or $\frac{1}{2}\pi$ then the $\mathbb{Z}_2$ discrete symmetry, under which the Higgs basis fields $H_1 \to +H_1$ and $H_2 \to -H_2$, is exact (and cannot be softly-broken[8]).

As an aside, we note that the so-called Inert Doublet Model (IDM) [41–43] can be defined as a Type I 2HDM with $Z_6 = Z_7 = 0$ [11], in which all fields (excepting H_2) are even under the $\mathbb{Z}_2$ discrete symmetry. In light of the above discussion, we see that the alignment limit is exact in the IDM and $\sqrt{2}H_1^0 - v$ is identified as the SM Higgs boson, which can either be the lighter or the heavier of the two CP-even Higgs bosons, depending on whether the inequality given in Eq. (9) is satisfied. The phenomenology of the IDM has been treated in detail in [44–46], so we do not pursue this case further in this paper.

Henceforth, we assume that $\sin 2\beta \neq 0$. The eight free parameters of the CP-conserving, softly-broken $\mathbb{Z}_2$-symmetric 2HDM are v, α, β, m_h, m_H, m_A, $m_{H^\pm}$ and m_{12}^2, where $0 < \beta < \frac{1}{2}\pi$ and $|\beta - \alpha| \leq \frac{1}{2}\pi$. The same counting can be performed in the Higgs basis. Note that the imposition of the discrete $\mathbb{Z}_2$ symmetry on the quartic terms of the scalar potential yields two relations among the Z_i as shown in [15, 18]

$$Z_2 = Z_1 + 2(Z_6 + Z_7)\cot 2\beta \,, \tag{37}$$

$$Z_3 = Z_1 - Z_4 - Z_5 + 2Z_6 \cot 2\beta - (Z_6 - Z_7)\tan 2\beta \,, \tag{38}$$

---

[7]Strictly speaking, if $\beta = \frac{1}{2}\pi$ then we need to interchange the Higgs basis fields H_1 and H_2 to be consistent with the definition of the Higgs basis specified in Eq. (1).

[8]Due to the potential minimum condition $Y_3 = -\frac{1}{2}Z_6 v^2$, it follows that $Z_6 = Z_7 = 0$ in the Higgs basis is sufficient to guarantee that the entire scalar potential respects the $\mathbb{Z}_2$ symmetry.

under the assumption[9] that $\beta \neq \frac{1}{4}\pi$. Thus, the eight independent parameters in the Higgs basis can be chosen as v, Y_2, Z_1, Z_3, Z_4, Z_5, Z_6, and β (with $0 < \beta < \frac{1}{2}\pi$) since Y_1 and Y_3 are determined by the scalar potential minimum conditions, and Z_2 and Z_7 can be determined from Eqs. (37) and (38). The parameter β serves to fix the $\mathbb{Z}_2$-basis relative to the Higgs basis. The translation between $\{Y_2, Z_1, Z_4, Z_5, Z_6\}$ and $\{m_h, m_H, m_A, m_{H^\pm}, \beta - \alpha\}$ is governed by Eqs. (3), (4) and (13)–(15). Specifying the parameter m_{12}^2 then allows one to determine Z_2, Z_3 and Z_7. In particular, it is convenient to introduce [cf. Eq. (36)],

$$\overline{m}^2 \equiv \frac{2m_{12}^2}{\sin 2\beta} = Y_2 + \tfrac{1}{2}Z_1 v^2 + Z_6 v^2 \cot 2\beta \,. \tag{39}$$

Using Eqs. (3), (4) and (38), it follows that

$$\overline{m}^2 = m_A^2 + Z_5 v^2 + \tfrac{1}{2}(Z_6 - Z_7)v^2 \tan 2\beta \,. \tag{40}$$

Combining the results of Eqs. (13)–(16) with Eq. (37), (38) and (40), we obtain,[10]

$$Z_2 v^2 = m_h^2(s_{\beta-\alpha} + 2c_{\beta-\alpha}\cot 2\beta)^2 + m_H^2(c_{\beta-\alpha} - 2s_{\beta-\alpha}\cot 2\beta)^2 - 4\overline{m}^2\cot^2 2\beta \,, \tag{41}$$

$$Z_3 v^2 = m_h^2 s_{\beta-\alpha}^2 + m_H^2 c_{\beta-\alpha}^2 + 2(m_h^2 - m_H^2)c_{\beta-\alpha}s_{\beta-\alpha}\cot 2\beta + 2(m_{H^\pm}^2 - \overline{m}^2) \,, \tag{42}$$

$$Z_7 v^2 = 2\big(m_h^2 c_{\beta-\alpha}^2 + m_H^2 s_{\beta-\alpha}^2 - \overline{m}^2\big)\cot 2\beta + (m_h^2 - m_H^2)s_{\beta-\alpha}c_{\beta-\alpha} \,. \tag{43}$$

Note that the following conditions are necessary (although not sufficient) to guarantee that the scalar potential in the Higgs basis is bounded from below [8, 41];

$$Z_1 > 0 \,, \qquad Z_2 > 0 \,, \qquad Z_3 > -\sqrt{Z_1 Z_2} \,. \tag{44}$$

The condition $Z_1 > 0$ is automatically satisfied in light of Eq. (13). The constraints on Z_2 and Z_3 imposed by Eq. (44) place mild constraints on the Higgs parameters employed in our numerical scans.

Finally, we examine the trilinear Higgs self-couplings, focusing on those involving the H. Explicit expressions for these couplings in terms of the Z_i and $\beta - \alpha$ have been given in [15]. The corresponding three-Higgs vertex Feynman rules (including the corresponding symmetry factor for identical particles but excluding an overall factor of i) are given by

$$g_{HHH} = -3v\big[Z_1 c_{\beta-\alpha}^3 + Z_{345}c_{\beta-\alpha}s_{\beta-\alpha}^2 - 3Z_6 s_{\beta-\alpha}c_{\beta-\alpha}^2 - Z_7 s_{\beta-\alpha}^3\big] \,, \tag{45}$$

$$g_{Hhh} = -3v\big[Z_1 c_{\beta-\alpha}s_{\beta-\alpha}^2 + Z_{345}c_{\beta-\alpha}\big(\tfrac{1}{3} - s_{\beta-\alpha}^2\big) - Z_6 s_{\beta-\alpha}(1 - 3c_{\beta-\alpha}^2) - Z_7 c_{\beta-\alpha}^2 s_{\beta-\alpha}\big] \,, \tag{46}$$

$$g_{HAA} = -v\big[(Z_3 + Z_4 - Z_5)c_{\beta-\alpha} - Z_7 s_{\beta-\alpha}\big] \,, \tag{47}$$

$$g_{HH^+H^-} = -v\big[Z_3 c_{\beta-\alpha} - Z_7 s_{\beta-\alpha}\big] \,, \tag{48}$$

where we have introduced the notation,

$$Z_{345} \equiv Z_3 + Z_4 + Z_5 \,. \tag{49}$$

---

[9]For $\beta = \frac{1}{4}\pi$, Eq. (38) implies that $Z_6 = Z_7$, in which case Z_3 must be considered as an independent quantity.

[10]The Higgs basis parameter Z_2 only appears in the quartic Higgs couplings, which we do not address in this paper. We only provide Eq. (41) for the sake of completeness.

In the alignment limit $|s_{\beta-\alpha}| \to 0$, Eqs. (17) and (45) yield:

$$g_{HHH} = g_{HHH}^{\rm SM} \left[1 - \frac{2Z_6}{Z_1} s_{\beta-\alpha} + \left(\frac{Z_{345}}{Z_1} - \frac{2Z_6^2}{Z_1^2} - \frac{3}{2} \right) s_{\beta-\alpha}^2 + \mathcal{O}(s_{\beta-\alpha}^3) \right], \qquad (50)$$

where the self-coupling of the SM Higgs boson is given by

$$g_{HHH}^{\rm SM} = -\frac{3m_H^2}{v} = -3v \left(Z_1 - Z_6 \frac{s_{\beta-\alpha}}{c_{\beta-\alpha}} \right). \qquad (51)$$

It is convenient to make use of Eq. (22) [in a convention where $c_{\beta-\alpha} \geq 0$] to write

$$s_{\beta-\alpha} = -\eta Z_6, \qquad (52)$$

where

$$\eta \equiv \frac{v^2}{\sqrt{(m_H^2 - m_h^2)(Z_1 v^2 - m_h^2)}} \qquad (53)$$

is a positive $\mathcal{O}(1)$ parameter. In the approach to the alignment limit, Eqs. (11) and (12) yield

$$\eta = \frac{v^2}{|m_A^2 + (Z_5 - Z_1)v^2|} + \mathcal{O}(Z_6^2). \qquad (54)$$

Inserting Eq. (52) in Eq. (50) yields

$$g_{HHH} = g_{HHH}^{\rm SM} \left\{ 1 + \left[(Z_{345} - \tfrac{3}{2}Z_1)\eta^2 + 2\eta \right] \frac{Z_6^2}{Z_1} + \mathcal{O}(Z_6^3) \right\}. \qquad (55)$$

In light of Eqs. (38) and (49), the parameter Z_{345} depends on Z_6. We can therefore rewrite Eq. (55) as

$$g_{HHH} = g_{HHH}^{\rm SM} \left\{ 1 + \left[(Z_7 \tan 2\beta - \tfrac{1}{2}Z_1)\eta^2 + 2\eta \right] \frac{Z_6^2}{Z_1} + (2\cot 2\beta - \tan 2\beta)\eta^2 \frac{Z_6^3}{Z_1} + \mathcal{O}(Z_6^3) \right\}, \quad (56)$$

where the term designated by $\mathcal{O}(Z_6^3)$ contains no potential enhancements in the limit of $s_{2\beta} \to 0$ or $c_{2\beta} \to 0$. The HHH coupling can thus be either suppressed or enhanced with respect to the SM. For example $g_{HHH} > g_{HHH}^{\rm SM}$ is possible in two cases. If $\tan\beta \sim 1$, then one must satisfy $(Z_7 - Z_6)\eta \tan 2\beta \gtrsim \tfrac{1}{2}Z_1\eta - 2$. Alternatively, if $\tan\beta \gg 1$, then one must satisfy $Z_6\eta \cot 2\beta \gtrsim \tfrac{1}{4}Z_1\eta - 1$. In both cases, the HHH coupling is enhanced even when $|Z_6|$ is significantly smaller than 1.

Next, consider the Hhh and HAA couplings given in Eqs. (46) and (47). Both these couplings approach nonzero values in the alignment limit $(s_{\beta-\alpha} \to 0)$,

$$g_{Hhh} = -vZ_{345} + \mathcal{O}(s_{\beta-\alpha}), \qquad (57)$$

$$g_{HAA} = -v(Z_{345} - 2Z_5) + \mathcal{O}(s_{\beta-\alpha}). \qquad (58)$$

One can now eliminate Z_{345} in favor of Z_6 as before. After employing Eq. (17), we end up with

$$g_{Hhh} = -\frac{1}{v} \left\{ m_H^2 - (Z_6 - Z_7)v^2 \tan 2\beta + 2Z_6 v^2 \cot 2\beta + \mathcal{O}(Z_6) \right\}, \qquad (59)$$

9

where the term designated by $\mathcal{O}(Z_6)$ contains no potential enhancements in the limit of $s_{2\beta} \to 0$ or $c_{2\beta} \to 0$.

Last but not least, it is noteworthy that

$$g_{HH^+H^-} = -vZ_3 + \mathcal{O}(s_{\beta-\alpha}), \tag{60}$$

approaches a finite nonzero value in the alignment limit. This is relevant for the analysis of the loop-induced process $H \to \gamma\gamma$, which has a contribution that is mediated by a $H^\pm$ loop. Recall that the charged Higgs mass is given by Eq. (25), which cannot be much heavier than $\mathcal{O}(v)$. Hence, the charged Higgs loop is parametrically of the same order as the corresponding SM loop contributions, thereby leading to a shift of the effective $H\gamma\gamma$ coupling from its SM value. This is in stark contrast to the behavior of tree-level Higgs couplings, which approach their SM values in the alignment limit.

Although we expect $m_{H^\pm} \lesssim \mathcal{O}(v)$ over most of the 2HDM parameter space when H is a SM-like Higgs boson, there exists a parameter regime [cf. Eqs. (27) and (28)] in which $m_{H^\pm} \gg m_H$. Indeed, a heavy charged Higgs mass is required in Type II to avoid conflict with the observed rate for $b \to s\gamma$ [47]. In light of Eqs. (3) and (4), suppose that $Y_2 \ll Z_3 v^2$ where Z_3 is large [say, of $\mathcal{O}(10)$] but still consistent with the unitarity bounds. In order to satisfy the inequality given in Eq. (9), $Z_4 + Z_5$ must be negative and its magnitude must be large (but not too large in order to satisfy the unitarity bounds). It then follows that $m_{H^\pm}^2 \simeq \frac{1}{2}Z_3 v^2$, in which case Eq. (48) yields

$$g_{HH^+H^-} \simeq -\frac{2m_{H^\pm}^2}{v} + \mathcal{O}(s_{\beta-\alpha}), \tag{61}$$

in the approach to the alignment limit.

One can also obtain Eq. (61) by expressing $g_{HH^+H^-}$ in terms of the Higgs masses and the squared-mass parameter $\overline{m}^2$ defined in Eq. (39). Inserting Eqs. (42) and (43) into Eq. (48) yields [15, 48]

$$g_{HH^+H^-} = -\frac{1}{v}\left\{ \left[m_H^2 + 2(m_{H^\pm}^2 - \overline{m}^2)\right]c_{\beta-\alpha} - 2\cot 2\beta (m_H^2 - \overline{m}^2)s_{\beta-\alpha}\right\}. \tag{62}$$

In the alignment limit where $c_{\beta-\alpha} \to 1$ (or equivalently, $Z_6 \to 0$),

$$g_{HH^+H^-} = -\frac{1}{v}(m_H^2 + 2m_{H^\pm}^2 - 2\overline{m}^2) + \mathcal{O}(s_{\beta-\alpha}), \tag{63}$$

where $m_H \simeq 125$ GeV. In the parameter regime where $m_{H^\pm}$ is large [such that $Y_2 \ll Z_3 v^2$ as discussed above Eq. (61)], it follows from Eq. (39) that $\overline{m}^2 \sim \mathcal{O}(v^2)$.[11] Thus, in the alignment limit with $m_{H^\pm}$ large compared to v, one again obtains the asymptotic result of Eq. (61).

We denote the one-loop $H \to \gamma\gamma$ amplitude normalized to the corresponding SM value by C_γ^H. The coupling given in Eq. (61) matches precisely the HH^+H^- interaction term of

$$\mathcal{L}_{\text{int}} = -\frac{gm_t}{2m_W}\bar{t}tH + gm_W W_\mu^+ W^{\mu-} H - \frac{gm_{H^\pm}^2}{m_W}H^+H^-H, \tag{64}$$

---

[11]If $|\cot 2\beta| \gg 1$, it is more convenient to invoke Eqs. (9) and (40) to conclude that $\overline{m}^2 \sim \mathcal{O}(v^2)$.

given in Eq. (2.15) of [6]. Hence, we can immediately obtain an estimate for C_γ^H in the alignment limit by employing the asymptotic forms for the contributions to the $H \to \gamma\gamma$ amplitude, F_i (corresponding to a particle in the loop with spin $i = 0, \frac{1}{2}, 1$) given in Eq. (2.21) of [6],

$$C_\gamma^H = \frac{F_0 + F_1 + 3e_t^2 F_{1/2}}{F_1 + 3e_t^2 F_{1/2}} \simeq 0.94, \tag{65}$$

where $e_t = \frac{2}{3}$ is the charge of the top quark in units of e, $F_0 = -\frac{1}{3}$, $F_{1/2} = -\frac{4}{3}$ and $F_1 = 7$.[12] A more complete calculation taking into account finite-mass effects yields a very similar result, $C_\gamma^H \simeq 0.95$. That is, the contribution of the charged Higgs loop asymptotically yields a 5% reduction in C_γ^H.

In contrast, in the case of lighter charged Higgs boson masses (which are allowed in Type I), the approximate form for the HH^+H^- coupling given in Eq. (61) and the asymptotic form for F_0 employed in Eq. (65) are no longer valid. In particular, in the approach to the alignment limit, $g_{HH^+H^-} \simeq -vZ_3$. When $Z_3 > 0$ [as in Eq. (61) where $Z_3 \sim 2m_{H^\pm}^2/v^2$], the charged Higgs loop interferes destructively with the W boson loop. However, for small values of $m_{H^\pm}$ there exist regions of the 2HDM parameter space where $Z_3 < 0$ [consistent with the bounds given in Eq. (44)], which then yields an HH^+H^- coupling of the opposite sign. In this case, the charged Higgs boson loop interferes constructively with the W boson loop, thereby generating a value of $C_\gamma^H > 1$. Using Eq. (63), it follows that the sign flip of $g_{HH^+H^-}$ occurs roughly when $2\overline{m}_{12}^2 > 2m_{H^\pm}^2 + m_H^2$. In practice, as we shall see in Section 3, positive values of $\overline{m}^2$ do not exceed about $(150 \text{ GeV})^2$, which implies that a light charged Higgs boson with a mass of about $m_{H^\pm} < 160$ GeV is required for $C_\gamma^H > 1$. The non-decoupling of the charged Higgs contribution and the possible sign flip in $g_{HH^+H^-}$ was also addressed in Appendix B of [49].

3 Numerical results

Let us now turn to the numerical scan of the 2HDM parameter space. The free parameters in our analysis are the four physical Higgs masses $m_h, m_H, m_{H^\pm}, m_A$, the squared-mass parameter m_{12}^2, the ratio of the two Higgs vacuum expectation values $\tan\beta$ and the mixing angle α of the CP-even Higgs squared-mass matrix. Setting $m_H \equiv 125.5$ GeV,[13] we allow the 2HDM parameters to vary in the following ranges

$$\alpha \in [-\pi/2, \pi/2], \quad \tan\beta \in [0.5, 60], \quad m_{12}^2 \in [-(2000 \text{ GeV})^2, (2000 \text{ GeV})^2],$$

$$m_h \in [10 \text{ GeV}, 121.5 \text{ GeV}], \quad m_{H^\pm} \in [m^*, 2000 \text{ GeV}], \quad m_A \in [5 \text{ GeV}, 2000 \text{ GeV}], \tag{66}$$

where m^* is the lower bound on the charged Higgs mass in Type I or Type II. Note that, as in [15], the degenerate case $m_h \simeq m_H$ is not considered in this study. Instead, we require a 4 GeV mass splitting between h and H in order to avoid h contamination of the H signal. Since we are primarily interested in the near-alignment case, we allow at most a 1% deviation

---

[12]These asymptotic forms are valid when $4m_i^2/m_H^2 \gg 1$, where m_i is the mass of the particle in the loop. Nevertheless, these approximations work quite well even for the t-quark and the W boson.

[13]Having performed the parameter scans before the publication of [50] which reports a central value of the Higgs mass of 125.09 GeV, we use 125.5 GeV as the observed Higgs mass in this analysis.

from $|C_V^H| = 1$, which translates into $|s_{\beta-\alpha}| \lesssim 0.14$. We also note that although the scan was performed in terms of α and $\tan\beta$ as given in Eq. (66), we will present our results in the convention of $c_{\beta-\alpha} \geq 0$. That means, given a point $(\alpha, \tan\beta)$ in our scan with $c_{\beta-\alpha} < 0$, we convert to the positive $c_{\beta-\alpha}$ convention by making the replacement $\alpha \to \alpha + \pi$ [see also the discussion around Eq. (34)]. Thus our alignment condition translates into $c_{\beta-\alpha} \geq 0.99$ whereas $s_{\beta-\alpha}$ can have either sign.

As in [15], the public tools used include 2HDMC [51] for computing couplings and decay widths and for testing theoretical constraints in the 2HDM, Lilith 1.1.2 [52] (with database version 15.04) for evaluating the Higgs signal strength constraints, and SusHi-1.3.0 [53] and VBFNLO-2.6.3 [54] for computing production cross sections at the LHC. The setup of the analysis and the experimental constraints imposed are exactly the same as in [15], with three additions. First, we include the recent update of the bound on the charged Higgs mass in Type II, $m_{H^\pm} > 480$ GeV at 95% CL [47], based on the observed rates for the weak radiative B-meson decay, $\overline{B} \to X_s\gamma$. Second, we take into account the new CMS result [17] on the search for a new heavy resonance decaying to a Z boson and a light resonance, followed by $Z \to \ell^+\ell^-$ and the light resonance decaying to $b\bar{b}$ or $\tau\tau$. In particular, the cross section upper limit for the $\ell\ell b\bar{b}$ final state in the plane of the masses of the two resonances, Fig. 5b of [17], puts a very severe constraint on $gg \to A \to Zh$ with $Z \to \ell\ell$ and $h \to b\bar{b}$ in our study.[14] This is in contrast to the $m_h \simeq 125$ GeV case studied in [15], where this limit has almost no effect. There are two reasons for the larger impact in the $m_H \simeq 125$ GeV, $c_{\beta-\alpha} \geq 0.99$ scenarios studied here: first, the ZAh coupling is proportional to $c_{\beta-\alpha}$ and therefore BR($A \to Zh$) is typically large; second, BR($h \to b\bar{b}$) ≈ 1 since the h is always light. Finally, the CMS constraint [16] on neutral Higgs bosons with masses between 25 GeV and 80 GeV, produced in association with a pair of b quarks, followed by the decay into $\tau\tau$, is also applied in our analysis. We find that this constraint eliminates a substantial part of the Type II parameter space at large $\tan\beta$. Unless otherwise stated, all parameter space points shown in the following satisfy all of the latest constraints. For more details on the numerical procedure, we refer the reader to [15].

3.1   Parameters

We start by illustrating the parameter space of the analysis. Figure 1 shows the relation between m_h, $|s_{\beta-\alpha}|$ and $\log_{10}|Z_6|$.[15] The expected correlation between the three parameters is clearly observed. In particular, larger values of m_h imply smaller $|Z_6|$ for the same value of $|s_{\beta-\alpha}|$, and for each m_h, $\log_{10}|Z_6|$ can be as small as desired if $|s_{\beta-\alpha}|$ is allowed to be correspondingly small. Here, we show results down to $|s_{\beta-\alpha}| = 10^{-5}$; we have checked that this catches all the phenomenology of the scenarios under consideration. Because of the absence of a

---

[14]The corresponding ATLAS search for $A \to Zh$ with $Z \to \ell\ell$ and $h \to b\bar{b}$ (or $\tau\tau$) [55] assumes a SM-like h with 125 GeV mass and thus does not apply here. (It would apply to $A \to ZH$ in our study, but does not give any relevant constraint for this case.)

[15]In this and subsequent figures, we give 3d information on a 2d plot by means of a color code in the third dimension. To this end, we must chose a definite plotting order. Ordering the points from high to low values in the third dimension, as done for $\log_{10}|Z_6|$ in Fig. 1, means that the highest values are plotted first and lower and lower values are plotted on top of them. As a consequence, regions with low values may (partly) cover regions with high values. The opposite is of course true for the ordering from low to high values. To avoid a proliferation of plots, in each figure we show only one ordering, trying to choose the one that gives most information. The figures with inverted plotting order are available upon request.
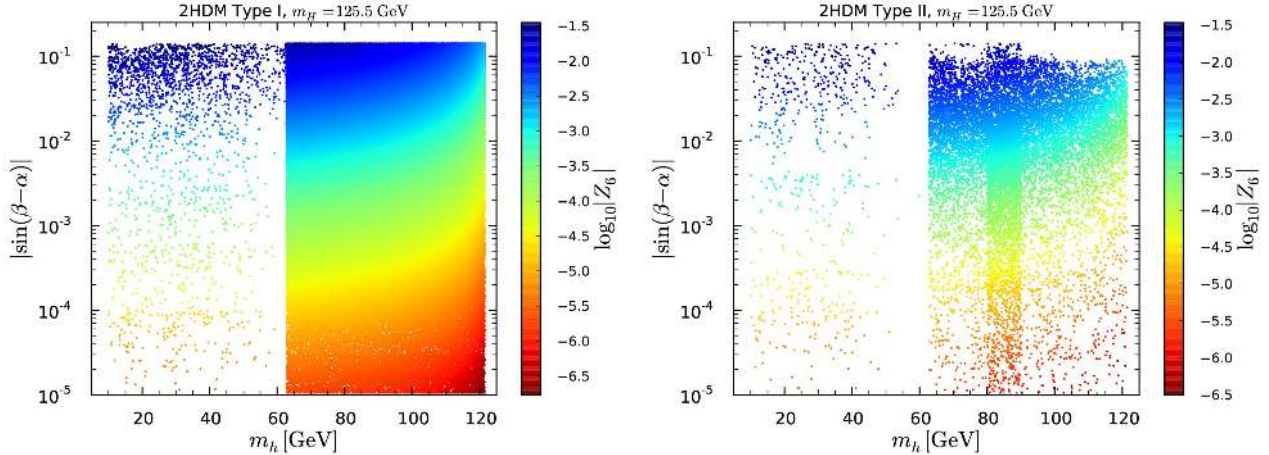
Figure 1: $|s_{\beta-\alpha}|$ versus m_h in Type I (left) and Type II (right) with $\log_{10}|Z_6|$ color code. Points are plotted in the order of high to low $\log_{10}|Z_6|$ values.

decoupling limit, $|Z_6|$ does not exceed $\sim 10^{-1.5}$ in our scan. This illustrates that in the scenario under consideration, alignment is solely controlled by the smallness of $|Z_6|$. Note also that the region of $m_h \leq \frac{1}{2}m_H$ requires subtle correlations among the 2HDM parameters to ensure that $\mathrm{BR}(H \to hh)$ is sufficiently small to be in agreement with the experimental constraints [56]. This explains the relatively low density of points in this region. On the other hand, the higher density of points seen in Type II for $m_h \in [80~\mathrm{GeV}, 90~\mathrm{GeV}]$ arises because light neutral states $X = h, A$ with masses below 80 GeV are severely constrained by the CMS $b\bar{b}X$ with $X \to \tau\tau$ search [16],[16] while masses above 90 GeV are also constrained by the ATLAS [58] and CMS [59] searches for $X \to \tau\tau$ decays in both the $gg \to X$ and $b\bar{b}X$ production modes.

The relation between the three free Higgs masses, m_A, $m_{H^\pm}$ and m_h is shown in Fig. 2. The absence of a decoupling limit results in an upper bound on the CP-odd and charged Higgs masses, $m_A, m_{H^\pm} \lesssim 630$ GeV, which depends on the allowed values of $c_{\beta-\alpha}$. Indeed, without the $c_{\beta-\alpha} \geq 0.99$ constraint that we imposed to focus on the alignment scenario, one would find instead $m_A, m_{H^\pm} \lesssim 800$ GeV, where the bound is saturated for $s_{\beta-\alpha} \simeq 0.7$ [49]. The characteristic correlation between m_A and $m_{H^\pm}$ is a consequence of the precision electroweak measurements, primarily the T parameter [60]. In Type II, a large part of the parameter space is excluded by weak radiative B meson decays for which agreement with observations sets a strong lower bound on the charged Higgs mass, $m_{H^\pm} > 480$ GeV at 95% CL, which is practically independent of $\tan\beta$ for $\tan\beta > 2$, and is even stronger for $\tan\beta < 2$ [47]. This constraint, in association with the distinctive m_A–$m_{H^\pm}$ correlation, sets a bound on the CP-odd Higgs mass. We find that $m_A \gtrsim 420$ GeV, which rules out the region of $m_A \leq \frac{1}{2}m_H$ in Type II. We also note that this forces the CP-odd and charged Higgs states to be relatively close in mass.

In contrast to Type II, the charged Higgs mass is much less impacted from flavor physics constraints [7,61] in Type I. For $m_{H^\pm} \lesssim 160$ GeV, the CP-odd state can have any mass below 630 GeV in Type I, as shown in the left panel in Fig. 2. Moreover, whereas $m_h \leq \frac{1}{2}m_H$ can only be found for $m_A, m_{H^\pm} \gtrsim 400$ GeV in Type II, such a light h is possible for most of

---

[16]The CMS analysis given in [16] considers only $pp \to b\bar{b}A$ production with $A \to \tau\tau$. However, the same limit should also apply to $pp \to b\bar{b}h$ with $h \to \tau\tau$; see *e.g.* [57].
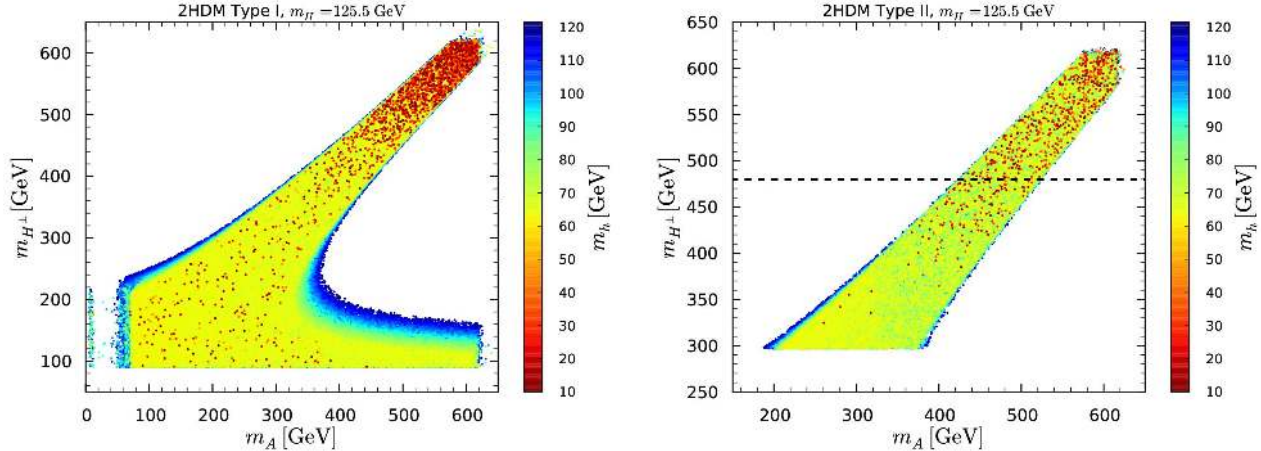
Figure 2: $m_{H^\pm}$ versus m_A in Type I (left) and Type II (right) with m_h color code. Points are ordered from high to low m_h values. The right plot shows the whole parameter space scanned over for Type II, with the horizontal line indicating the updated limit on the charged Higgs mass, $m_{H^\pm} > 480$ GeV.

the allowed combinations of m_A and $m_{H^\pm}$ in Type I—with the notable exception of the light $m_A \leq \frac{1}{2} m_H$ region, since LEP constraints imply that A and h cannot both have a mass below $\frac{1}{2} m_H$ simultaneously [56]. However, there are narrow bands at the border of the allowed m_A vs. $m_{H^\pm}$ region that unambiguously lead to values of $m_h \gtrsim 100$ GeV. One such region is the blue band in the left panel of Fig. 2 with $m_A \gtrsim 350$ GeV and $m_{H^\pm} \lesssim 200$ GeV. Such mass correlations may be used to predict or cross-check the validity of the scenario in the case that two or three extra Higgs states are discovered in the future. Finally, as discussed in [56], m_h values below about 60 GeV are only possible for $\tan\beta \lesssim 2$ in Type II. Hence, if such a low mass h is observed and its properties require a high value of $\tan\beta$, then the Type II model would be eliminated.

3.2 Couplings

Let us now turn to the properties of the H in the (near-)alignment regime. Figure 3 shows the possible variation of the coupling of H to up-type fermions, $C_U^H = C_D^H \equiv C_F^H$ in Type I and C_U^H in Type II. Deviations from unity of around $\pm 10\%$ are possible in Type I for $|s_{\beta-\alpha}| \sim 0.14$, while in Type II the deviations range from -7% to $+20\%$. As expected, in both types C_U^H quickly approaches unity as $|s_{\beta-\alpha}|$ decreases. It is interesting to note that, while $C_U^H = \sin\alpha/\sin\beta$ in both Type I and Type II, the actual values that can be reached are different in the two models because of constraints involving the down-type coupling. The largest deviations occur for large h–A mass splitting, when m_h is below 60 GeV, while m_A is close to its upper bound. As discussed in [56], $\tan\beta$ is very close to 1 in this case. In Type I, there is also another region with $m_h < \frac{1}{2} m_H$ at larger values of $\tan\beta$, although this is only achieved when $|s_{\beta-\alpha}| \gtrsim 10^{-2}$. This is seen as the narrow banana-shaped red strip with $C_F \approx 1$–1.01 in the upper left panel of Fig. 3. Also noteworthy are the white gaps between the regions filled with valid scan points: these are caused by the CMS limits [17] on $A \to Zh \to \ell\ell b\bar{b}$ (and
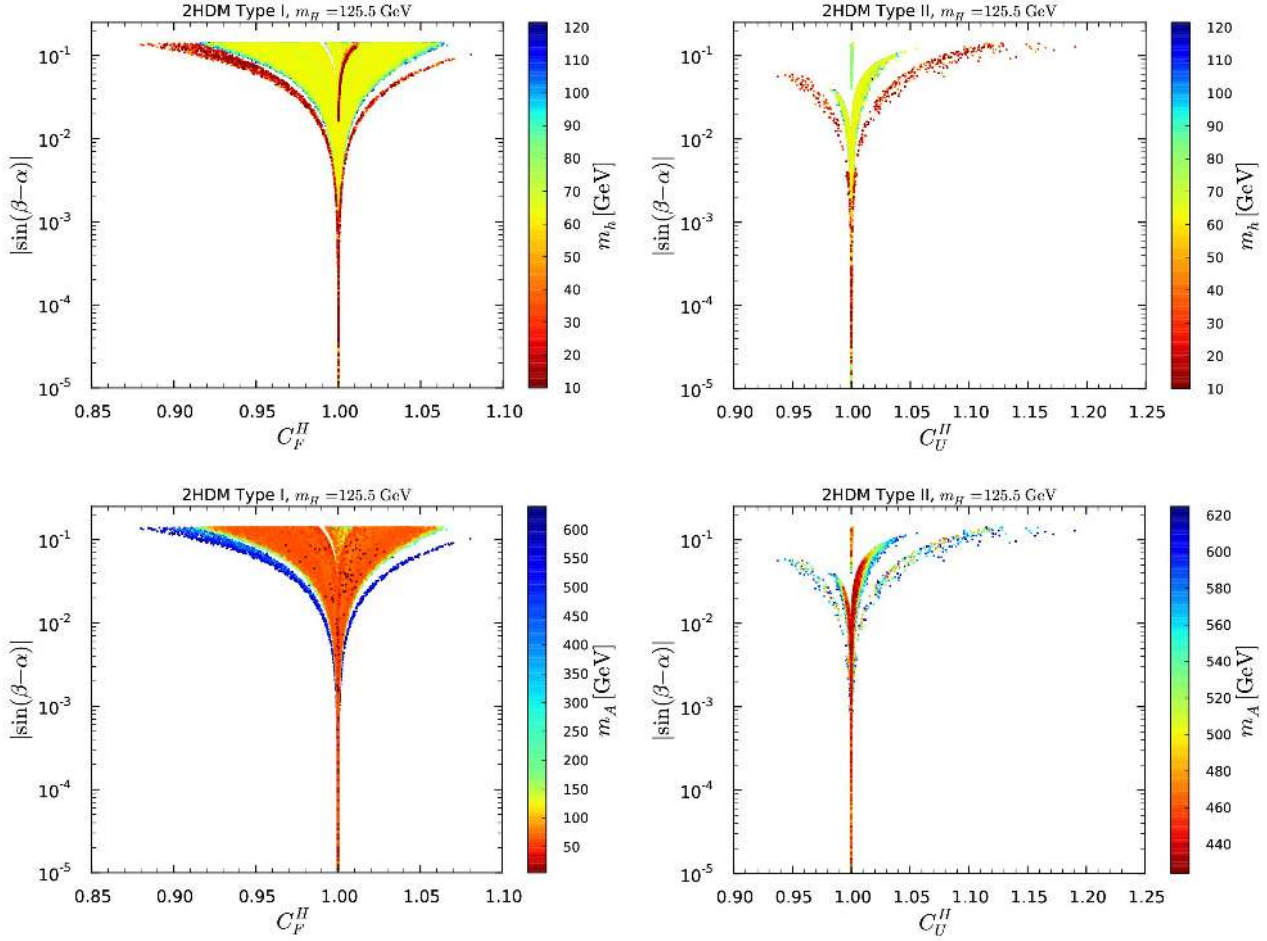
Figure 3: $|s_{\beta-\alpha}|$ versus reduced fermionic coupling C_F^H in Type I (left) and C_U^H in Type II (right). In the upper two panels, the color code shows the dependence on m_h; in the lower two panels the dependence on m_A, with points ordered from high to low m_h and m_A values, respectively. Note that the color scales for m_A are different for Type I and Type II because of the very different allowed ranges of m_A.

$\ell\ell\tau\tau$) and will appear in many of the subsequent figures. The impact of this limit is discussed in more detail in the Appendix.

The possible variation of the coupling to down-type fermions, C_D^H, in Type II is shown in Fig. 4. Let us first consider the left panel. As in the $m_h = 125$ GeV case, there are two solutions: one where C_V^H, C_U^H and C_D^H all have the same sign (as is the case in the SM), and one where C_D^H has opposite sign relative to C_U^H and C_V^H [48]. In the normal (same) sign region, deviations from the predicted SM coupling in the range of roughly -30% to $+12\%$ are possible even for rather low $|s_{\beta-\alpha}| \sim 5 \times 10^{-3}$, as long as the $H \to hh$ decay mode is closed. If the $H \to hh$ decay (which is constrained to BR($H \to hh$) $\lesssim 0.27$ at 95% CL by the fit to the 125 GeV signal strength measurements) contributes to the total width, then C_D^H is confined to the range $[0.83, 1.08]$ and quickly converges to unity as $|s_{\beta-\alpha}|$ decreases. Note however that C_D^H is never exactly 1 unless $|s_{\beta-\alpha}|$ is at the level of few times 10^{-3} or smaller. The gap between

15
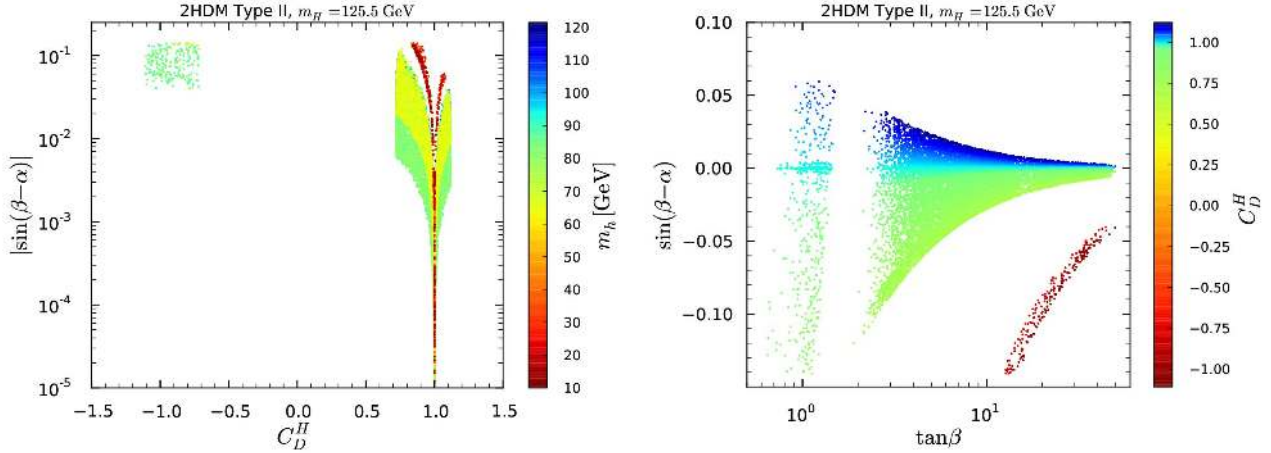
Figure 4: In the left panel, we exhibit $|s_{\beta-\alpha}|$ versus C_D^H in Type II. The color code shows the dependence on m_h, with points ordered from high to low m_h values. In the right panel, we exhibit $s_{\beta-\alpha}$ vs. $\tan\beta$ with the color code showing C_D^H ordered from high to low values.

the red and the yellow/green/blue points is again caused by the CMS limits on $A \to Zh$. On the other hand, the opposite-sign region, $C_D^H \in [-1.1, -0.7]$, requires $s_{\beta-\alpha} \lesssim -0.04$ due to the fact that $s_{\beta-\alpha}$ and $\tan\beta$ are correlated in Type II as illustrated in the right panel of Fig. 4. We see that $C_D^H = c_{\beta-\alpha} + s_{\beta-\alpha} t_\beta \gtrsim 1$ for $s_{\beta-\alpha} \gtrsim 0$ but decreases below 1 when $s_{\beta-\alpha}$ turns negative. Consequently, for moderately negative $s_{\beta-\alpha}$ and large enough $\tan\beta$, C_D^H flips sign. Values of $|C_D^H| \lesssim 0.7$ are excluded by the fit of the signal strengths, but the opposite-sign solution with $C_D^H \approx -1$ is still phenomenologically viable. The region of $\tan\beta \gtrsim 50$ is excluded because of the strong constraints on $A \to \tau\tau$ decays from ATLAS [58] and CMS [59]; see also [49]. The CP-odd scalar mass m_A does not have much influence, since it can only vary over the very limited range 420–630 GeV in Type II. Large deviations of C_D^H may imply large excursions of the H signal strengths away from 1, the details of which will be studied in Section 3.3.

The $\tan\beta$ dependence of the fermionic couplings, shown in Fig. 5, is also noteworthy. In both Type I and Type II, sizable deviations from $C_U^H = c_{\beta-\alpha} - s_{\beta-\alpha}/t_\beta = 1$ are possible only for small $\tan\beta$. In Type II, C_U^H very quickly converges to 1 once $\tan\beta \gtrsim 7$–8 because the allowed range of $s_{\beta-\alpha}$ decreases with increasing $\tan\beta$, as can be seen in the right panel of Fig. 4. In Type I, the convergence of the fermionic couplings to their SM values is less pronounced due to the fact that, even for $\tan\beta = 60$, the full $|s_{\beta-\alpha}|$ range considered is allowed. For C_D^H in Type II, the situation is quite different, as this coupling is given by $\cos\alpha/\cos\beta$ instead of $\sin\alpha/\sin\beta$. For the normal-sign region, as soon as $\tan\beta$ is at least moderate in size ($\tan\beta \approx 10$), C_D^H saturates the full range allowed by the measured signal strengths, even for small values of $|s_{\beta-\alpha}|$ of a few times 10^{-3}. In contrast, as discussed in the previous paragraph, the opposite-sign solution is only possible for large enough negative $s_{\beta-\alpha}$, concretely $s_{\beta-\alpha} \lesssim -0.04$, cf. the right panel of Fig. 4. Overall, in these plots, the impact of the CMS limit on $A \to Zh$ is even more striking than in Fig. 3, as it excludes most points with $\tan\beta \approx 1.2$–1.8 in Type I and the entire range of $\tan\beta \approx 1.5$–2 in Type II.

Turning to the loop-induced Higgs couplings to gluons and to photons, we first note that the H coupling to gluons, C_g^H, is dominated by the top-quark loop, and its behavior is thus
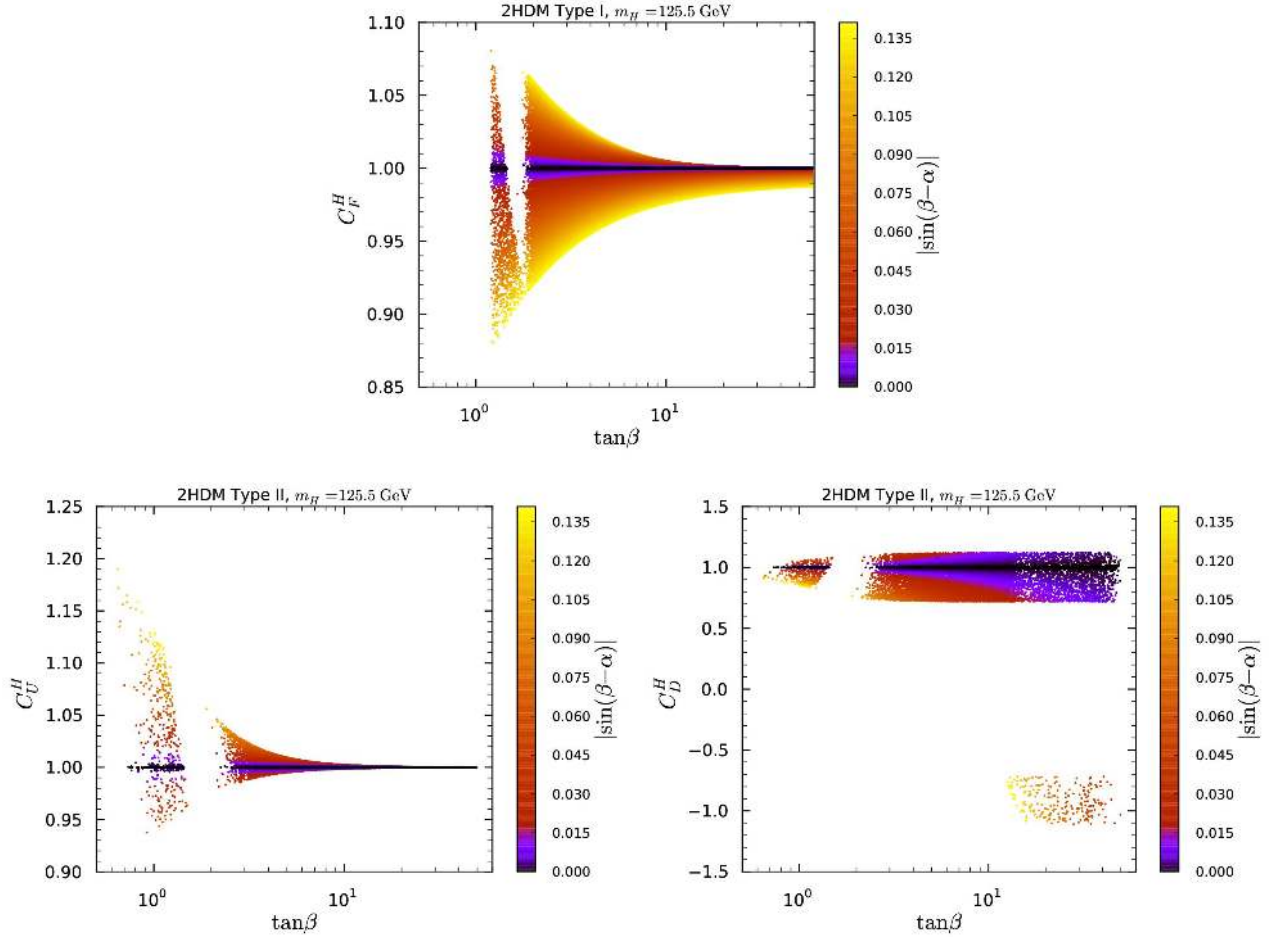
Figure 5: Fermionic couplings versus $\tan\beta$ in Type I (upper panel) and Type II (lower panels) with $|s_{\beta-\alpha}|$ color code. Points are ordered from high to low $|s_{\beta-\alpha}|$.

practically the same as that of C_U^H in Figs. 3 and 5. We therefore do not show separate plots for C_g^H. However, an exception occurs for the opposite-sign C_D^H solution, for which the b-loop contribution interferes constructively with the t-loop contribution, resulting in $C_g^H \approx 1.06$. (The same happens in the $m_h = 125$ GeV case, see [15, 48].)

The coupling to photons, C_γ^H, is more complicated. Here, the main contributions come from W and top-quark loops as in the SM, as well as from loops with charged Higgs bosons. The W and top-quark loops contribute with opposite signs, and thus the values of $C_U^H > 1$ ($C_U^H < 1$) seen in Fig. 3 will lead to smaller (larger) C_γ^H, respectively. The $H^\pm$ loop typically also has the opposite sign relative to the $W^\pm$ loop and can thus substantially suppress C_γ^H even at very small $s_{\beta-\alpha}$. (However, positive interference of the $W^\pm$ and $H^\pm$ loops is possible for low $m_{H^\pm}$, as noted at the end of Section 2.) The net effect on C_γ^H is shown in Fig. 6. In particular, we observe a large variation in C_γ^H in Type I, where the charged Higgs boson can be light. For $|s_{\beta-\alpha}| \lesssim 10^{-2}$ and $m_{H^\pm} \gtrsim 500$ GeV, we find $C_\gamma^H \approx 0.95$ in both Type I and Type II, in agreement with the expected 5–6% reduction of C_γ^H relative to the SM in the limit $|s_{\beta-\alpha}| \to 0$ with heavy $m_{H^\pm}$ [cf. Eq. (63)]. For $|s_{\beta-\alpha}| \gtrsim 10^{-2}$ (but still assuming that $m_{H^\pm}$ is

17
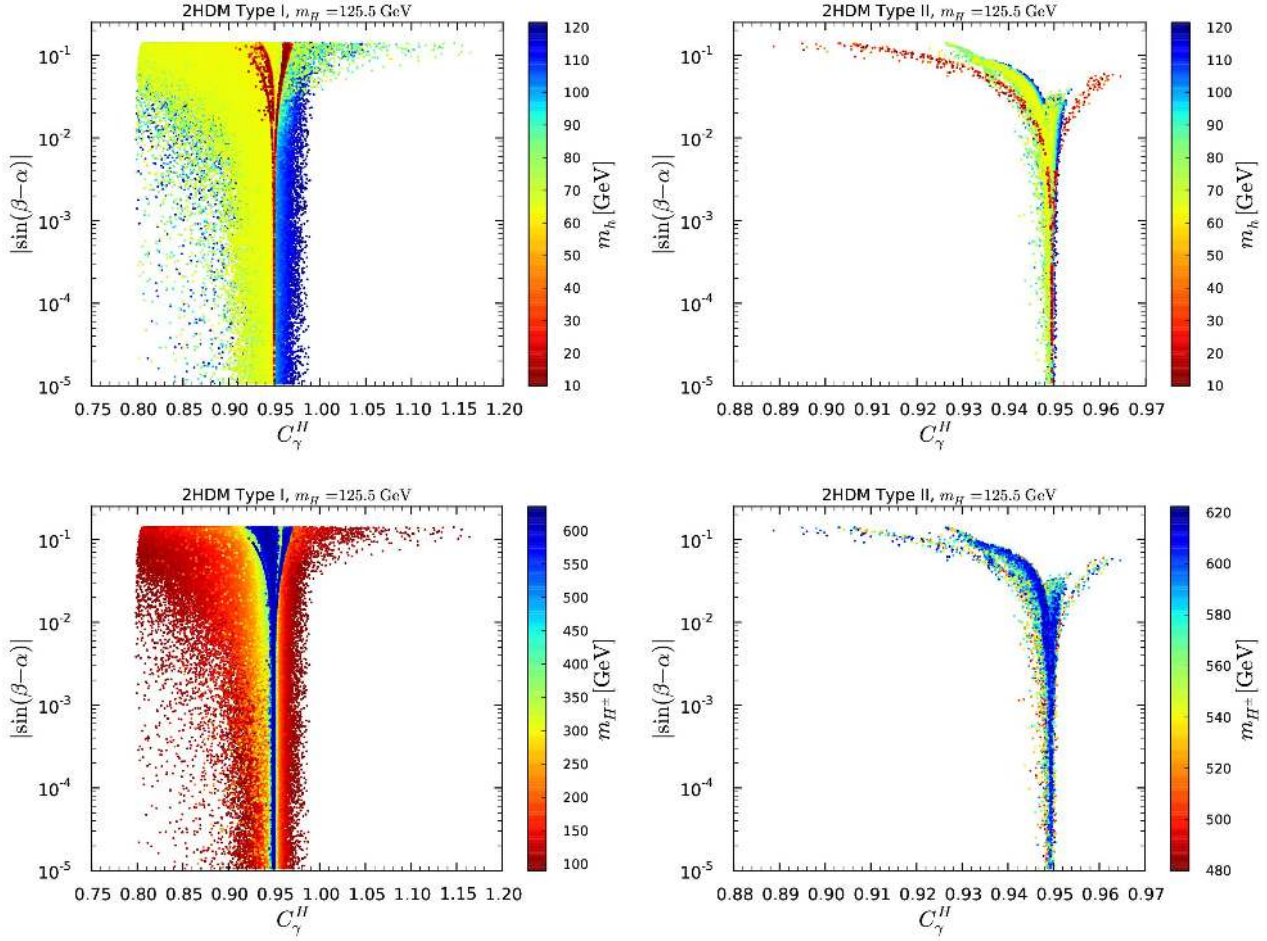
Figure 6: $|s_{\beta-\alpha}|$ versus C_γ^H in Type I (left) and Type II (right) with m_h color code (upper panels) and with $m_{H^\pm}$ color code (lower panels). Points are ordered from high to low m_h in the upper panels and from low to high $m_{H^\pm}$ in the lower panels.

large), this reduction can be more or less than 5% depending on the sign of $\overline{m}^2 \equiv 2m_{12}^2/\sin 2\beta$. Note however, that while $\overline{m}^2 < 0$ can reach values as large as $-(350\ \text{GeV})^2\ \left[-(200\ \text{GeV})^2\right]$ in Type I [Type II], respectively, $\overline{m}^2 > 0$ does not exceed $\sim (150\ \text{GeV})^2$. Therefore, in Type II where $m_{H^\pm} > 480$ GeV, C_γ^H is always below 1 (although one will need linear collider precision to pin this down with sufficient accuracy [62]). In contrast, in Type I, for $m_{H^\pm} \lesssim 160$ GeV a value of $\overline{m}^2$ between about $(60\ \text{GeV})^2$ and $(120\ \text{GeV})^2$ can lead to a switch in sign of $g_{HH^+H^-}$, giving $C_\gamma^H > 1$. The dependence on $\overline{m}^2$ is illustrated explicitly in Fig. 7. Of course such a light charged Higgs boson can also (and in fact more easily) suppress C_γ^H, down to $C_\gamma^H \approx 0.8$, irrespective of the value of $|s_{\beta-\alpha}|$.

Finally, we consider the trilinear HHH coupling, which is useful for consistency checks of the model, provided it can be measured precisely enough. The dependence of $C_{HHH} \equiv g_{HHH}/g_{HHH}^{\text{SM}}$ on $|s_{\beta-\alpha}|$ and m_h (top panels) as well as m_A (bottom panels) is shown in Fig. 8. Similar to C_{hhh} in the non-decoupling regime of the $m_h = 125$ GeV scenario [15], large values of the triple Higgs coupling beyond 1 can be achieved for $|s_{\beta-\alpha}|$ values of the order of 0.1 in the alignment regime

18
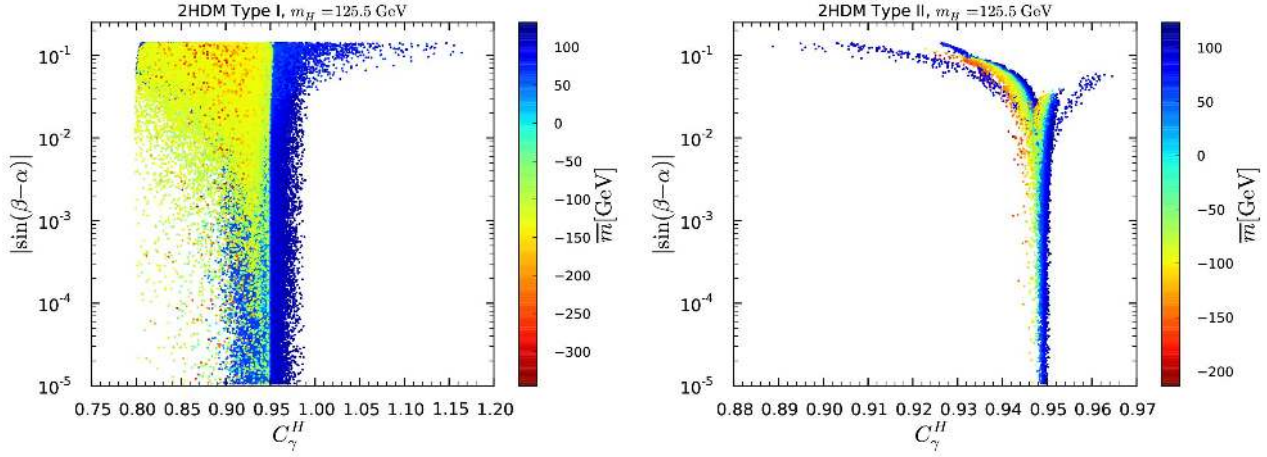
Figure 7: As for Fig. 6 but showing the dependence of C_γ^H on $\overline{m} \equiv \mathrm{sgn}\,\overline{m}^2 \sqrt{|\overline{m}^2|}$. Points are ordered from high to low $\overline{m}$.
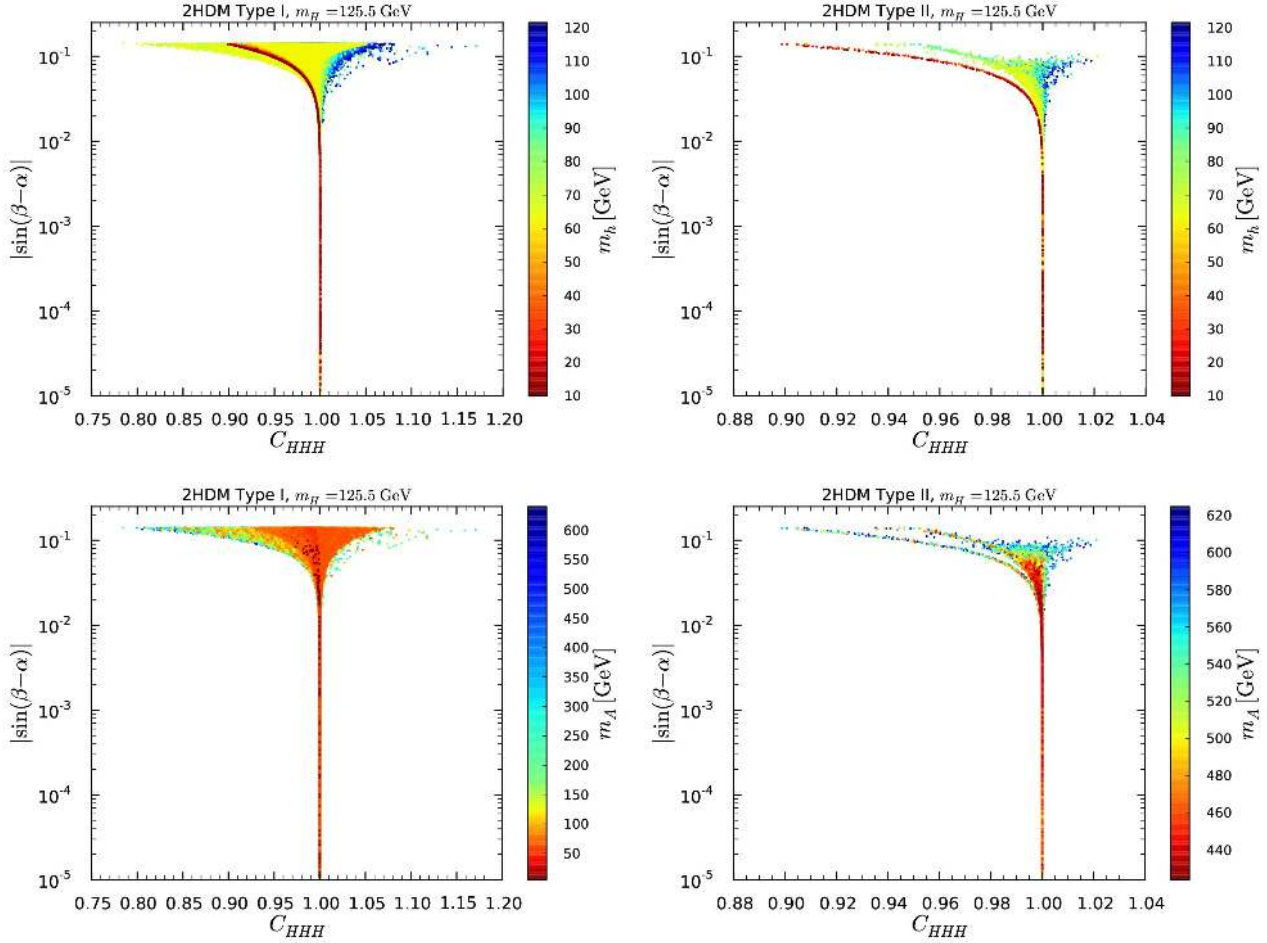
Figure 8: Reduced triple Higgs coupling C_{HHH} in Type I (left) and Type II (right), in the top panels with m_h and in the bottom panels with m_A color coding. Points are ordered from high to low $\overline{m}$, m_h or m_A values.
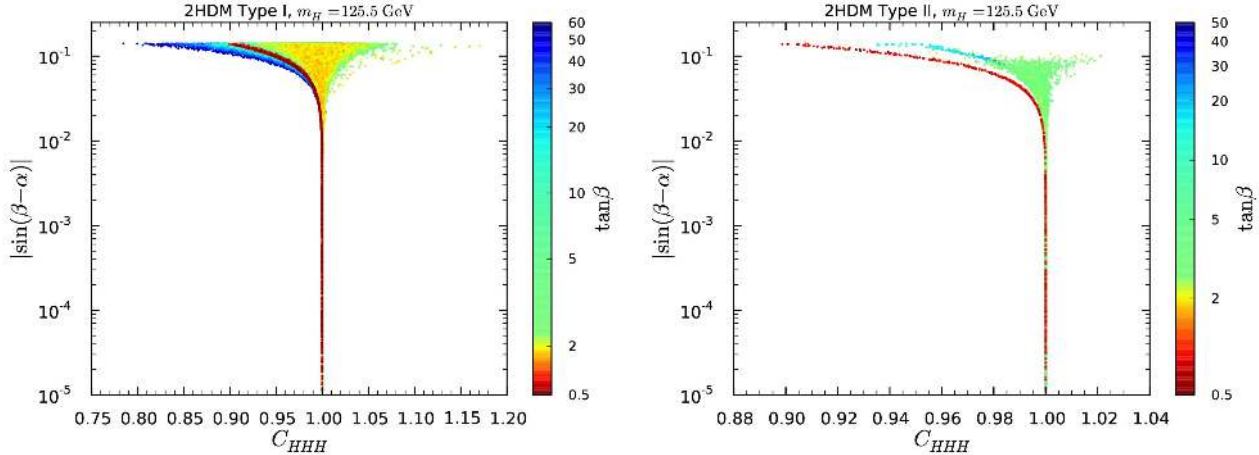
Figure 9: As in Fig. 8 but with $\tan\beta$ color coding. Points are ordered from high to low $\tan\beta$ values.

of the $m_H = 125$ GeV scenario. But, there is no direct analogue to the decoupling regime of the $m_h = 125$ GeV scenario, where the triple Higgs coupling was always suppressed as compared to its SM prediction. Instead, in the $m_H = 125$ GeV scenario, C_{HHH} can be enhanced or suppressed for any value of m_A. However, most of the points which might have had $C_{HHH} \gg 1$ are associated with $\tan\beta \approx 1$–2, which is precisely the range eliminated by the CMS limits on $gg \to A \to Zh$. In the end we are left with $C_{HHH} \approx 0.8$–1.2 in Type I and $C_{HHH} \approx 0.9$–1.02 in Type II.[17] In Type I, the possible variation is less important for smaller m_A, in particular for m_A below about 100 GeV. Moreover, we note that $C_{HHH} \leq 1$ for $m_h \lesssim 60$ GeV in both Type I and Type II. Finally, the smallest values of $C_{HHH} < 1$ in Type I are found for large $\tan\beta$, while in Type II C_{HHH} converges to 1 with increasing $\tan\beta$, as shown in Fig. 9.

3.3 Signal strengths

The variations in the couplings to fermions discussed above have direct consequences for the signal strengths of the SM-like Higgs boson. In Type I, the signal strengths in the $H \to \gamma\gamma$ decay mode are driven by the value of $m_{H^\pm}$, while for the $H \to VV^*$ ($VV^* = ZZ^*, WW^*$) and $H \to \tau\tau$ decay modes they depend mostly on C_F^H, as illustrated in Fig. 10.[18] Notice that the C_F^H dependence in the ZZ^* mode is opposite for gg fusion and vector boson fusion (VBF) production. In the case of VBF, a smaller value of C_F^H implies a smaller $b\bar{b}$ partial width and therefore a larger ZZ^* branching ratio, whereas in gg production C_F^H determines the size of the top-quark loop contribution which is enhanced for a larger value of C_F^H. In contrast, in Type II, the signal strengths are always dominantly driven by C_D^H, as this determines the $H \to b\bar{b}$ partial width (and $m_{H^\pm}$ is constrained to be heavy). This is illustrated in Fig. 11. In this case, the dependence is always the same for gg and VBF production.

Putting everything together we find quite distinct correlations of signal strengths as shown in Fig. 12 for Type I and in Fig. 13 for Type II. It is especially noteworthy that even in the

---

[17]Without the $gg \to A \to Zh$ limits, we find values up to $C_{HHH} \approx 1.4$, as discussed in Appendix A.

[18]We employ the notation $\mu_X^H(Y)$ for the signal strength in the production mode X and decay mode $H \to Y$.
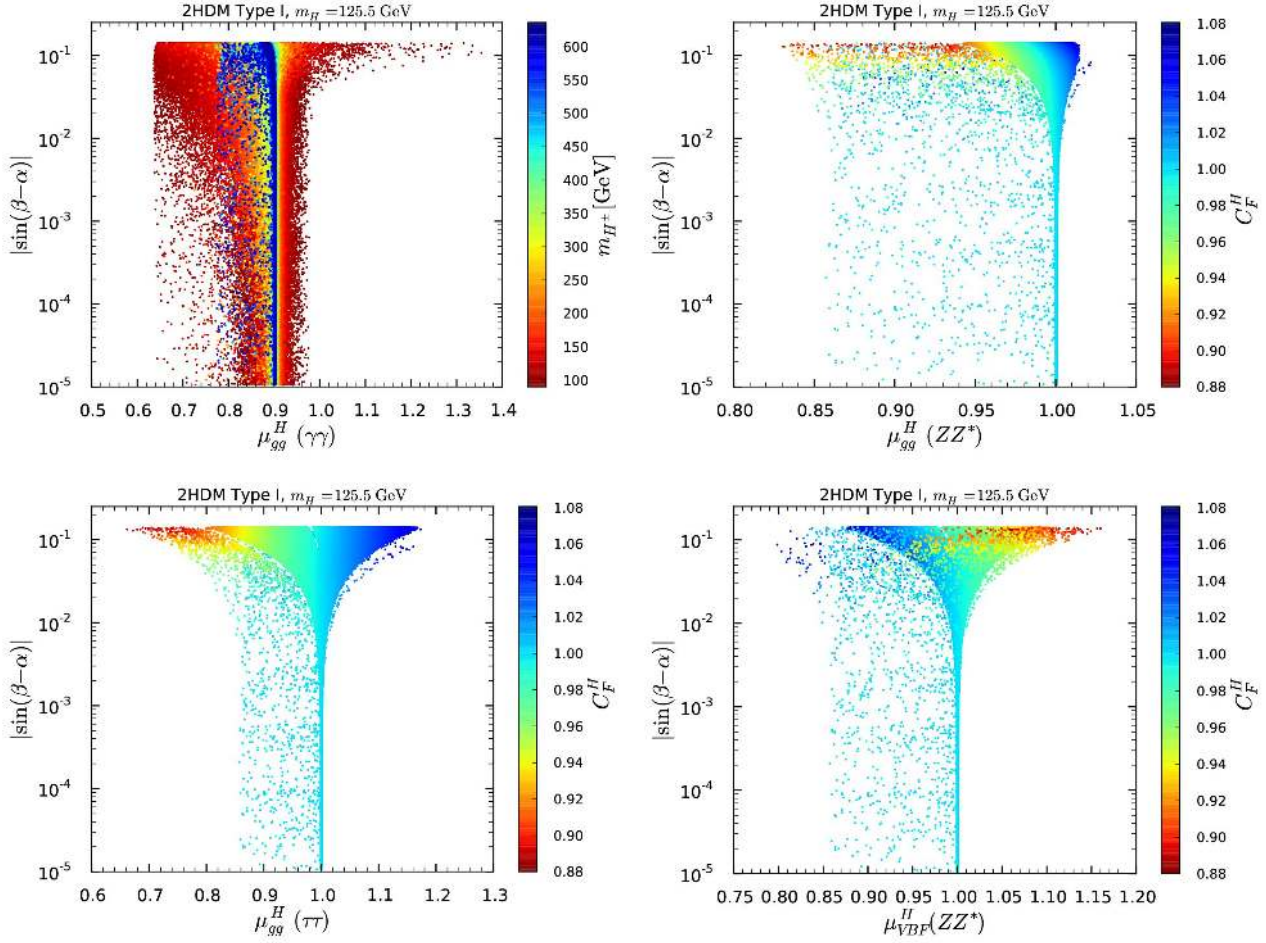
Figure 10: Signal strengths in Type I.

deep alignment limit, the signal strengths can significantly differ from the corresponding SM predictions, but the ratio of gg and VBF production is very close to 1. Moreover, certain combinations can only be reached for specific ranges of m_h and/or m_A values. For example, $\mu_{gg}^H(\gamma\gamma) \simeq \mu_{\mathrm{VBF}}^H(\gamma\gamma) \simeq 0.7$ requires $m_h \gtrsim 60$ GeV in Type I while it is not reached at all in Type II. Likewise, a suppression of $\mu_{gg}^H(\gamma\gamma)$ while $\mu_{\mathrm{VBF}}^H(\gamma\gamma) \gtrsim 1$ would point towards a somewhat heavy A in Type I with a slight departure from strict alignment, while again this combination is not possible in Type II. Another example is the relation between $\mu_{gg}^H(\gamma\gamma)$ and $\mu_{gg}^H(ZZ^*)$. In the alignment limit in Type II we expect $\mu_{gg}^H(\gamma\gamma)/\mu_{gg}^H(ZZ^*) \simeq 0.9$, with both enhancement or suppression of the individual $\mu_{gg}^H(\gamma\gamma), \mu_{gg}^H(ZZ^*)$ with respect to the SM being possible. In Type I, there is a band in which this ratio also applies (for all m_h) and the signals are always suppressed. For values of $m_h \gtrsim 60$ GeV in Type I, in the deep (near) alignment limit we find $\mu_{gg}^H(ZZ^*) \sim 1$ ($\in [0.95, 1.02]$), while $\mu_{gg}^H(\gamma\gamma)$ can range from 0.64 to 0.98 (1.4). An analogous discussion is possible for $\mu_{gg}^H(\tau\tau)$ versus $\mu_{gg}^H(\gamma\gamma)$.

In general, when $H \to hh$ or $H \to AA$ decays are kinematically allowed, these (so far) unobserved decay modes suppress the H branching ratios into SM final states, thus leading to a simultaneous suppression of all the $\mu_X^H(Y)$ even in the deep alignment regime. This is apparent in all the μ correlations shown in Figs. 12 and 13, but is most notably visible as the

21
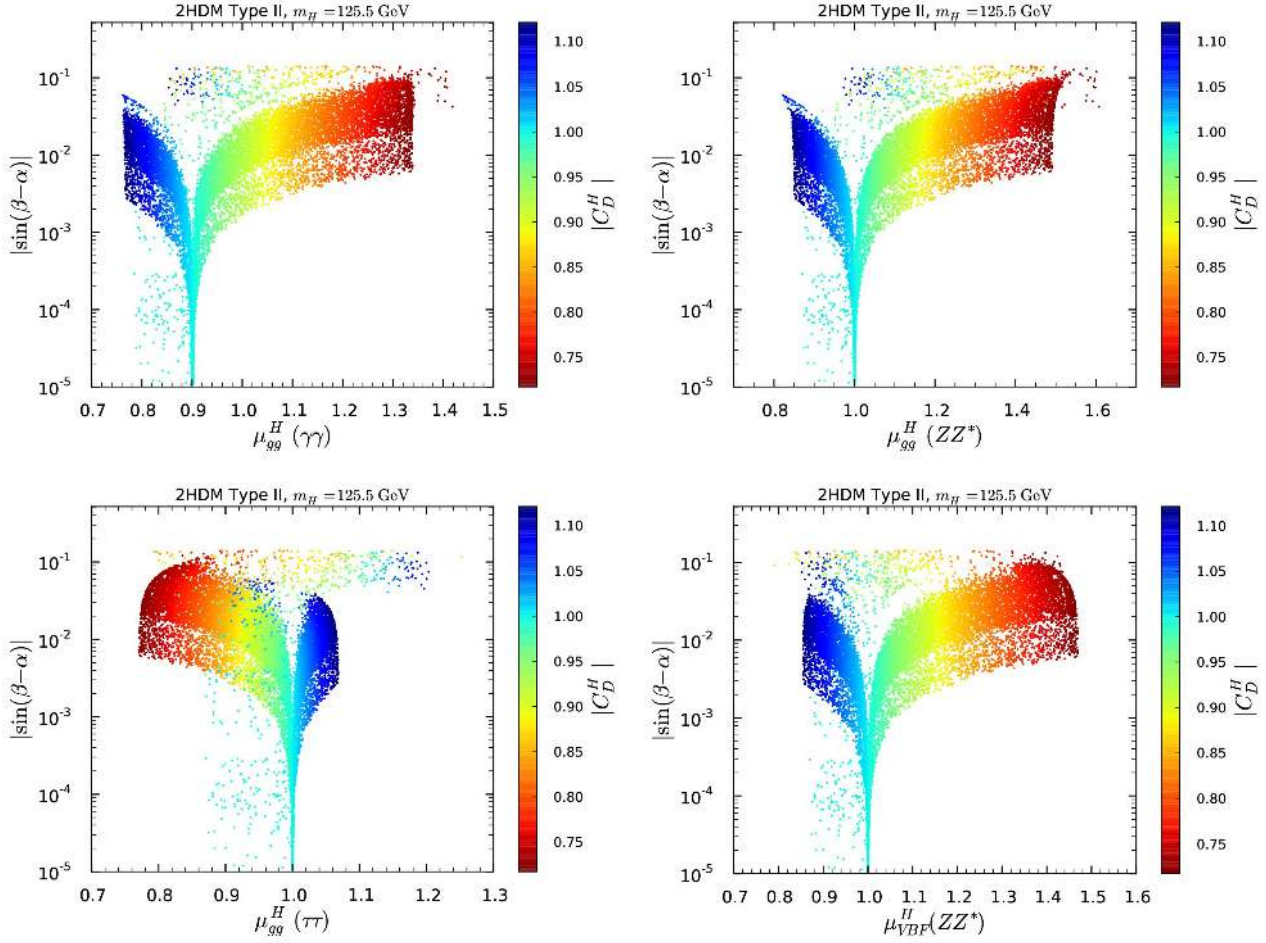
Figure 11: Signal strengths in Type II. The horizontal bars near $|s_{\beta-\alpha}| \approx 0.1$ arise from the opposite-sign C_D^H solution.

upward-sloping diagonal lines of points in the $\mu_{gg}^H(ZZ^*)$ vs. $\mu_{gg}^H(\gamma\gamma)$ and $\mu_{gg}^H(\tau\tau)$ vs. $\mu_{gg}^H(\gamma\gamma)$ plots for Type I. (However, note that in Type II due to the non-universal nature of the Yukawa couplings the signal strengths can also be larger than 1 when the $H \to hh$ decay mode is open.)

Comparing these results with the corresponding results of [15], it seems very difficult to distinguish $m_h \simeq 125$ GeV from $m_H \simeq 125$ GeV with signal strength measurements and coupling fits alone. One possibility for such a distinction might be that the measured values point towards Type I or Type II but are excluded by $A \to Zh$ in the case of $m_H \simeq 125$ GeV for a particular model type. Such a result would obviously favor the $m_h \simeq 125$ GeV scenario.
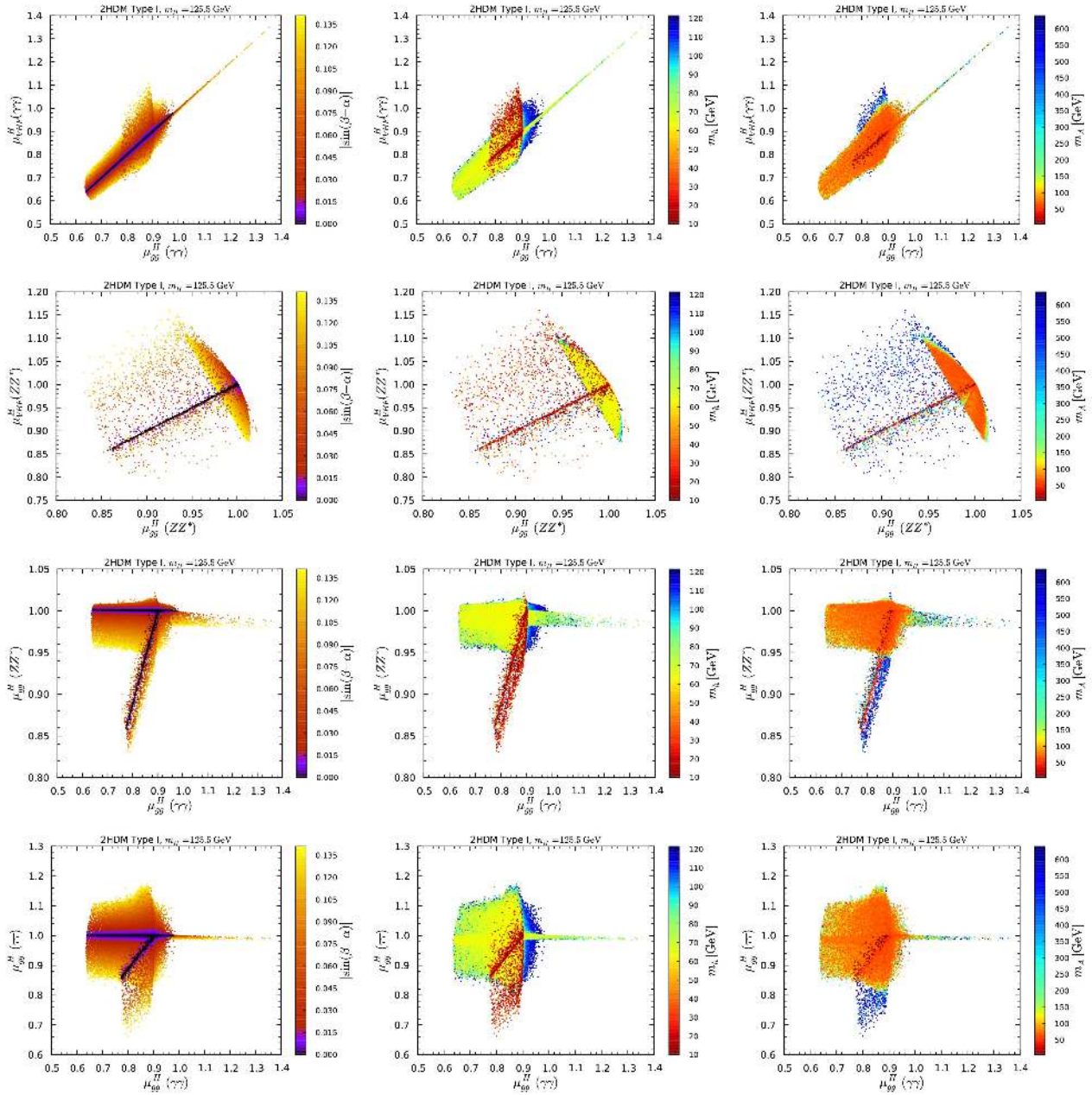
Figure 12: Examples of correlations between signal strengths in Type I. The top panels show $\mu_{\text{VBF}}^H(\gamma\gamma)$ vs. $\mu_{gg}^H(\gamma\gamma)$, the upper middle panels show $\mu_{\text{VBF}}^H(ZZ^*)$ vs. $\mu_{gg}^H(ZZ^*)$, the lower middle panels show $\mu_{gg}^H(ZZ^*)$ vs. $\mu_{gg}^H(\gamma\gamma)$ and the bottom panels show $\mu_{gg}^H(\tau\tau)$ vs. $\mu_{gg}^H(\gamma\gamma)$. The color code indicates, from left to right, the dependence on $|s_{\beta-\alpha}|$, m_h and m_A. Points are ordered from high to low $|s_{\beta-\alpha}|$, m_h and m_A values.
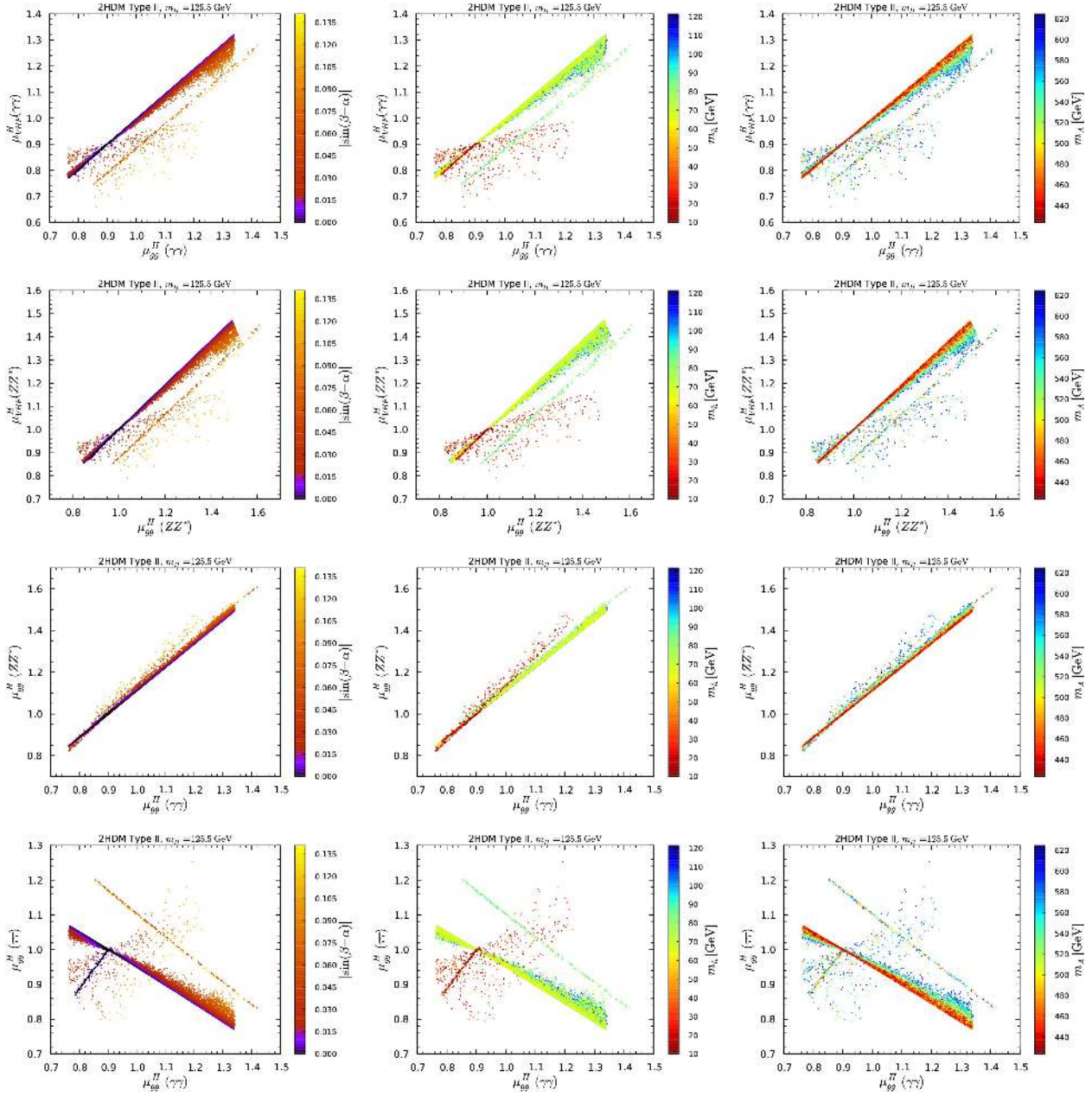
Figure 13: Examples of correlations between signal strengths in Type II. The top panels shows $\mu^H_{\text{VBF}}(\gamma\gamma)$ vs. $\mu^H_{gg}(\gamma\gamma)$, the upper middle panels show $\mu^H_{\text{VBF}}(ZZ^*)$ vs. $\mu^H_{gg}(ZZ^*)$, the lower middle panels show $\mu^H_{gg}(ZZ^*)$ vs. $\mu^H_{gg}(\gamma\gamma)$ and the bottom panels show $\mu^H_{gg}(\tau\tau)$ vs. $\mu^H_{gg}(\gamma\gamma)$. The color code indicates, from left to right, the dependence on $|s_{\beta-\alpha}|$, m_h and m_A. Points are ordered from high to low $|s_{\beta-\alpha}|$, m_h and m_A values. Note that the correlations look the same in the first two rows of plots (*i.e.* for VBF vs. gg production in $\gamma\gamma$ or ZZ^* final state) but the actual μ values are different. The opposite-sign C_D^H solution is visible as a separate narrow line with: $|s_{\beta-\alpha}| \approx 0.1$ (left-hand panels), $m_h \gtrsim 65$ GeV (middle panels) and $m_A \in [420, 630]$ GeV (right-hand panels).

3.4 Cross sections for h and A production

Let us now turn to the prospects for discovering the additional neutral scalar states. The two largest production modes at the LHC are gluon fusion, $gg \to X$, and the associated production with a pair of b-quarks, $b\bar{b}X$, with $X = h, A$. The correlations of the $gg \to X$ and $b\bar{b}X$ cross sections at the 13 TeV LHC are shown in Fig. 14 for the Type I model and in Fig. 15 for the Type II model. We show the points that pass all present constraints (in beige) and highlight those that have a very SM-like 125 GeV Higgs state by constraining all the following signal strengths to be within 5% or 2% of their SM values, respectively, denoted as SM±5% (red) and SM±2% (dark red):

$$\mu_{gg}^H(\gamma\gamma),\ \mu_{gg}^H(ZZ^*),\ \mu_{gg}^H(\tau\tau),\ \mu_{\mathrm{VBF}}^H(\gamma\gamma),\ \mu_{\mathrm{VBF}}^H(ZZ^*),\ \mu_{\mathrm{VBF}}^H(\tau\tau),\ \mu_{VH}^H(b\bar{b}),\ \mu_{t\bar{t}}^H(b\bar{b})\,. \tag{67}$$

Regarding the production of h and A in Type I, shown in Fig. 14, there is a strong correlation between the two production modes, gluon fusion and $b\bar{b}$ associated production, which stems from the fact that the relevant couplings are the same (up to a sign in the case of the A): $C_U^h = C_D^h = \cos\alpha/\sin\beta$ and $C_U^A = -C_D^A = \cot\beta$, respectively. The larger spread in $\sigma(b\bar{b}A)$ observed for $\sigma(gg \to A) > 10^{-2}$ pb comes from the fact that for $m_A \lesssim 400$ GeV the $b\bar{b}A$ cross section grows faster with decreasing m_A than that of $gg \to A$. Therefore, along a line of fixed $\sigma(gg \to A)$ in the plot, a point with higher $\sigma(b\bar{b}A)$ has a smaller m_A. Note also that there is an interference of the top and bottom loop diagrams in $gg \to A$ which changes sign depending on the value of m_A. However, $\sigma(gg \to A)$ is always at least two orders of magnitude larger than $\sigma(b\bar{b}A)$.

Turning to Type II scenarios, we observe that in the case of the A either the $b\bar{b}A$ or the $gg \to A$ cross section can be dominant due to the fact that the $Ab\bar{b}$ and $At\bar{t}$ couplings have different $\tan\beta$ dependence, the former being proportional to $\tan\beta$ and the latter to $\cot\beta$. Also, as already noted in [49], the $m_H \simeq 125$ GeV scenarios can be either eliminated or confirmed
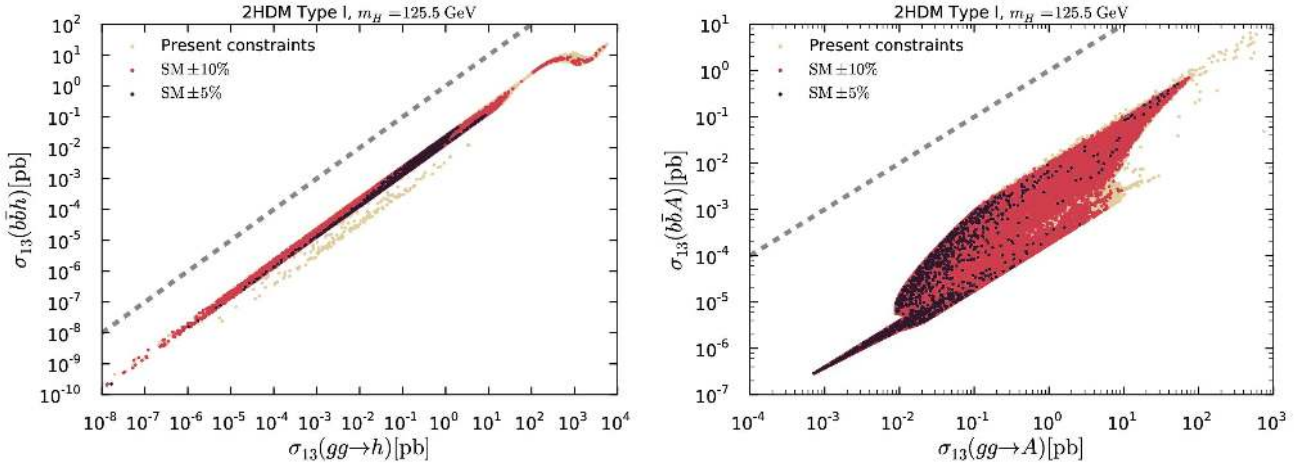

Figure 14: $\sigma(b\bar{b}X)$ versus $\sigma(gg \to X)$ for $X = h$ (left) and $X = A$ (right) in Type I at the 13 TeV LHC for points satisfying all present constraints (in beige) as well as points for which the signals strengths from Eq. (67) are within 5% and 2% of the SM predictions (in red and dark red, respectively). The dashed lines indicate $\sigma_{13}(b\bar{b}X) = \sigma_{13}(gg \to X)$.
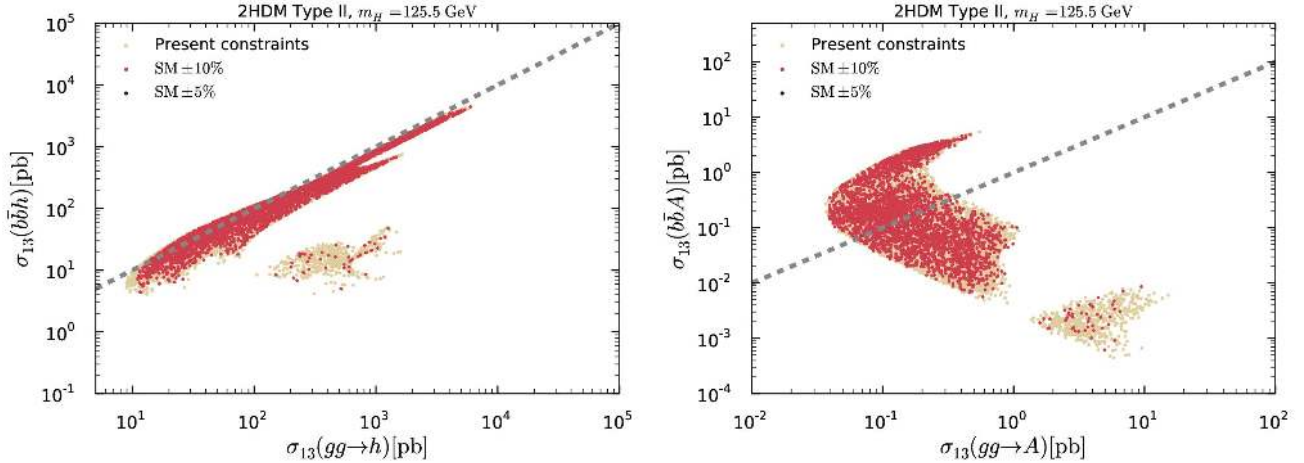
Figure 15: As in Fig. 14 but for Type II.

when the LHC measurements reach a precision such that the rates in the various initial×final state channels can be measured to 5% accuracy. This is because for this scenario the charged Higgs boson loop contribution to the $H\gamma\gamma$ coupling results in at least a 5% reduction in the $H \to \gamma\gamma$ coupling.

Before considering specific decay channels of h and A, we present in Fig. 16 the gluon-fusion cross sections, as well as the $b\bar{b}A$ cross section, as functions of m_h and m_A in Type I and Type II at the 13 TeV LHC. Here, the color code shows the dependence on $\tan\beta$. In Type I, the $gg \to A$ cross section is proportional to $\cot^2\beta$; this explains why it is larger (smaller) at lower (higher) $\tan\beta$. A cross section of 1 fb is guaranteed for m_A up to the maximum possible mass of ~ 600 GeV. At very small m_A and low $\tan\beta$ it can reach 100 pb. On the other hand, the $gg \to h$ cross section in Type I is proportional to $(C_F^h)^2$ and can take on extremely small values. The reason is that $s_{\beta-\alpha}$ can take either sign and the values allowed in our scan are high enough such that a cancellation between the two terms of $C_F^h = s_{\beta-\alpha} + c_{\beta-\alpha}\cot\beta$ can occur and leads to an almost vanishing coupling. For $m_h < \frac{1}{2}m_H$, this cancellation is also possible for fine-tuned points at large $\tan\beta$, but for most points $\tan\beta$ is small and the cross section can be as large as 5×10^3 pb at $m_h \sim 10$ GeV. In Type II, any phenomenologically viable mass in the range 420–630 GeV gives a $gg \to A$ cross section larger than 30 fb with values as large as 10 pb possible for $\tan\beta \lesssim 1$. Moreover, note that the $\tan\beta$ dependence is opposite for $b\bar{b}A$ compared to $gg \to A$ so that one or the other cross section is always large, as illustrated in the right panel of Fig. 15. As for h in Type II, the smallest $gg \to h$ cross section is of order 8 pb at $m_h \simeq 120$ GeV, with values as large as $4 - 6 \times 10^3$ pb for $m_h \sim 80 - 90$ GeV at very large $\tan\beta$. As previously mentioned, large values of $\tan\beta$ are excluded for $m_h < 80$ GeV and $m_h > 90$ GeV because of the severe constraints from $h \to \tau\tau$ decays. For values of $m_h < \frac{1}{2}m_H$, for which $\tan\beta$ must be small, the $gg \to h$ cross section takes a minimum value of ~ 100 pb reaching 2×10^3 pb at $m_h \sim 10$ GeV. To summarize, the prospects for observing the h are good in Type II, while the prospects for discovering the A look promising in both Type I and Type II.
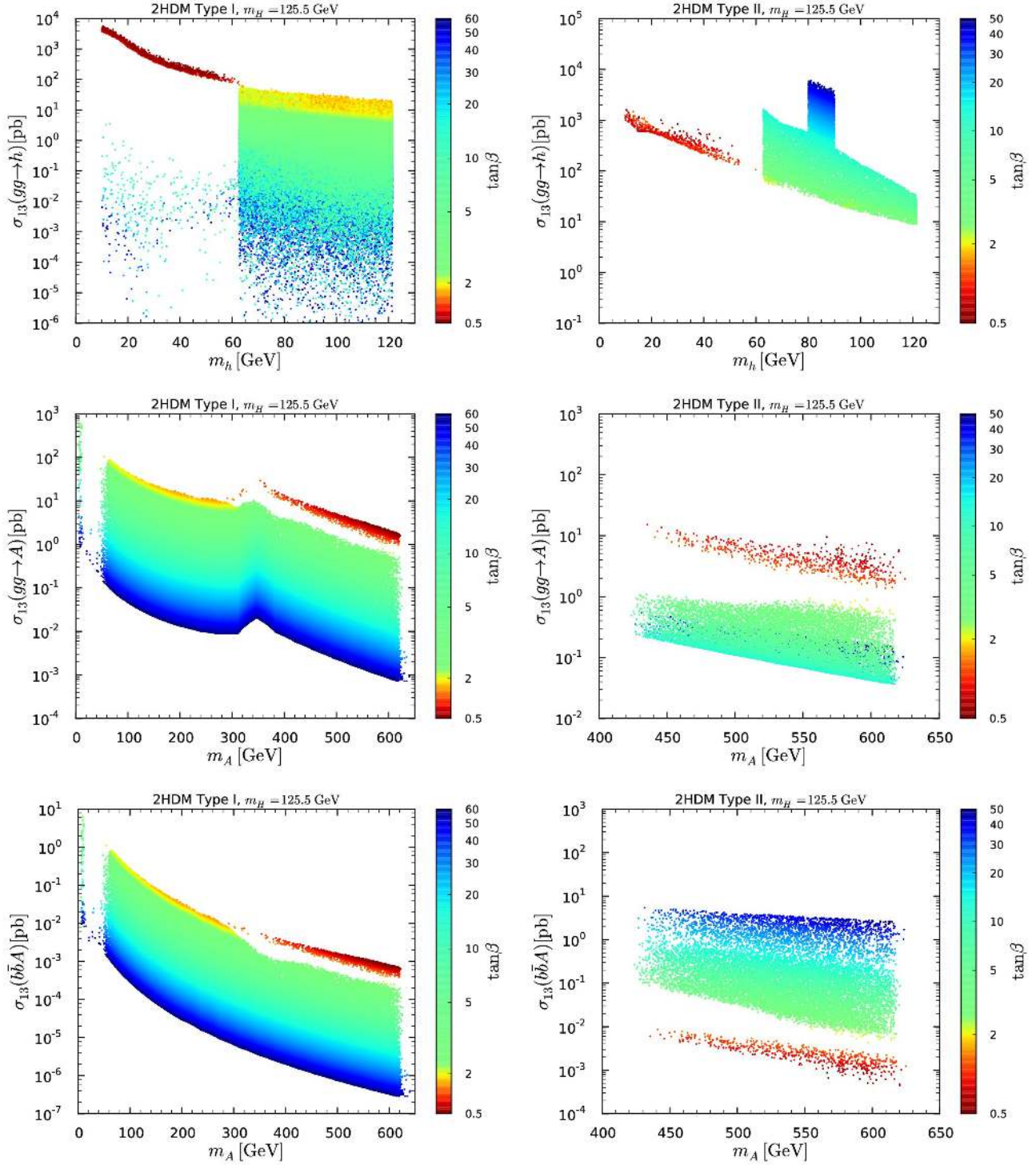
Figure 16: Cross sections in Type I (left) and Type II (right) for $gg \to X$ as functions of m_X for $X = h$ (upper panels) and $X = A$ (middle panels) with $\tan\beta$ color code. The bottom panels depict the cross sections for $b\bar{b}A$ production as function of m_A with $\tan\beta$ color code. In all six plots, points are ordered from high to low $\tan\beta$.
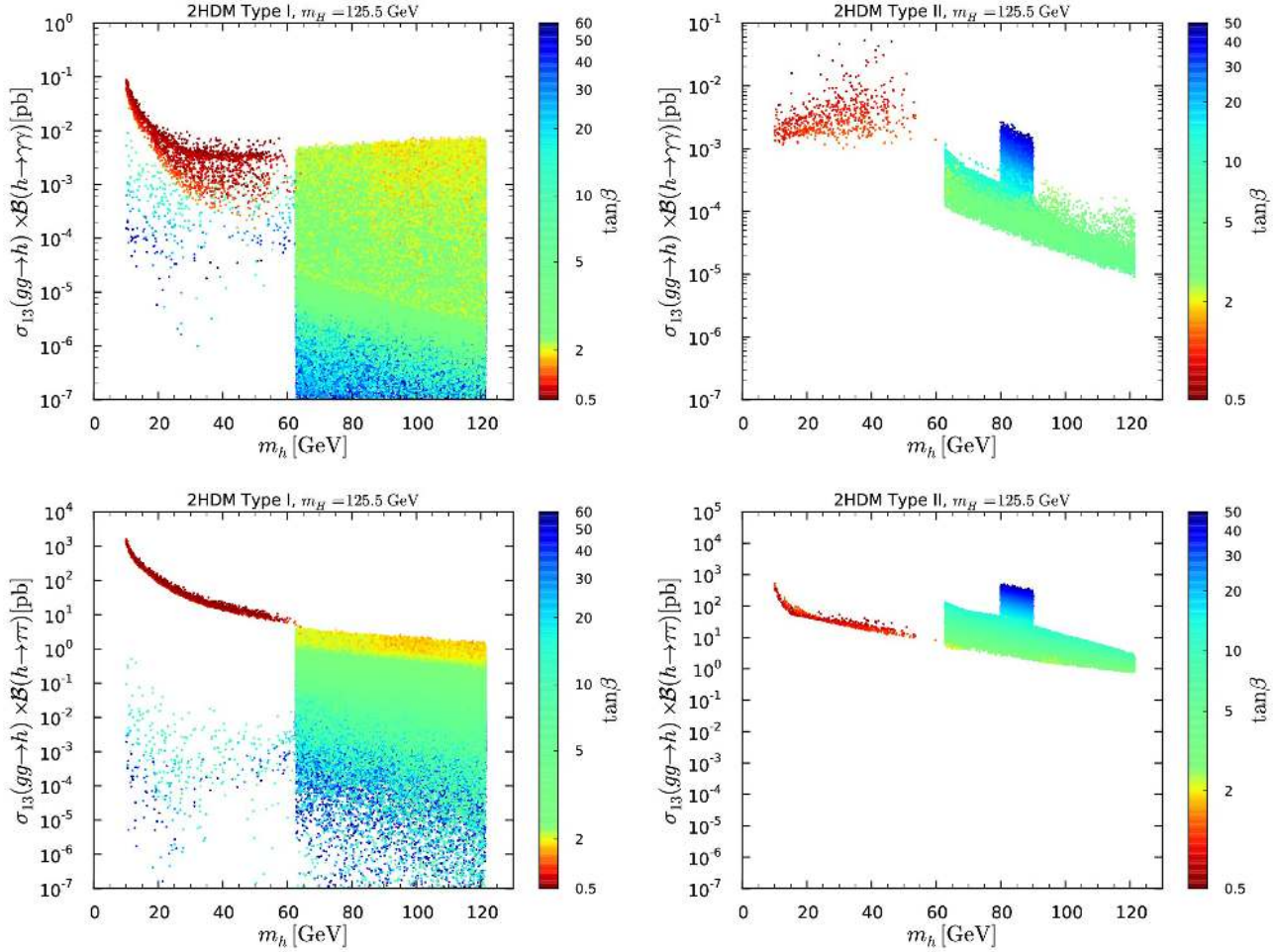
Figure 17: Cross sections times branching ratios in Type I (left) and in Type II (right) for $gg \to h \to Y$ at the 13 TeV LHC as functions of m_h for $Y = \gamma\gamma$ (upper panels) and $Y = \tau\tau$ (lower panels) with $\tan\beta$ color code. Points are ordered from high to low $\tan\beta$.

Let us now turn to specific signatures.[19] The cross sections for $gg \to h \to Y$ with $Y = \gamma\gamma$ and $\tau\tau$ in Types I and II are exhibited in Figure 17. Note that the y-axis is cut off at 10^{-7} pb. Although much lower values of the cross section are possible in some cases, we do not show these lower values since they will certainly not be observable at the LHC. In Type II, $gg \to h \to \gamma\gamma$ cross sections of at least 1 fb are guaranteed if $m_h < \frac{1}{2}m_H$. In this same region one finds that $\sigma(gg \to h \to \gamma\gamma) > 0.1$ fb in Type I if $\tan\beta < 2$. For $m_h \gtrsim \frac{1}{2}m_H$, cross sections in the $\gamma\gamma$ final state can reach 10 fb (3 fb) in Type I (Type II), though they can also be much lower, especially in Type I. The behavior of $\sigma(gg \to h \to \tau\tau)$ is similar with cross sections above 1 pb over the full m_h range in Type II, and also in Type I if $\tan\beta$ is small enough. Existing limits on $\sigma(gg \to h \to \gamma\gamma)$ at 8 TeV from CMS for $m_h = 80$–110 GeV are roughly 0.05–0.1 pb at 68% CL [63]. Thus, we expect that future Run 2 data will eventually provide a sensitive probe

---

[19]To avoid a proliferation of plots, we focus here primarily on the results for gluon fusion; all corresponding results for the $b\bar{b}$ cross section can be provided upon request.

in this channel, which will be particularly interesting if the analyses can be extended to cover the whole m_h range down to about 10 GeV.

The cross sections for A production with decays into SM channels, $A \to \gamma\gamma$, $\tau\tau$, $t\bar{t}$, are presented in Fig. 18. In Type I, the $gg \to A \to \gamma\gamma$ ($\tau\tau$) cross section can be as large as roughly 15 fb (10 to 1 pb), respectively, for $m_A \in [60, 200]$ GeV, with minimum values that would still be potentially observable for $m_A \lesssim 100$ GeV for a very large integrated luminosity. Of course, the maximal (minimal) values arise for small (large) $\tan\beta$, implying an indirect determination of $\tan\beta$ would be possible by measuring these cross sections. We also note a narrow band of non-excluded points with m_A between 10 and 60 GeV (cf. [56]), with very large $gg \to A \to \tau\tau$ cross sections for $m_A \sim 10$ GeV. For $m_A \in [200, 2m_t]$ the A cross section is small in both the $\gamma\gamma$ and $\tau\tau$ channels, and the $t\bar{t}$ cross section is either zero or very tiny. Once $m_A > 2m_t$, a very substantial $gg \to A \to t\bar{t}$ cross section (up to about 0.3 pb for $\tan\beta > 2$ and roughly 0.1–6 pb for $\tan\beta < 2$) is possible for small $\tan\beta$, but as $\tan\beta$ increases this cross section declines rapidly. Turning to Type II, we see that observation of the A in the $\gamma\gamma$ final state will be, at best, extremely difficult. In contrast, observation of $b\bar{b}A$ production with $A \to \tau\tau$ may be possible at large $\tan\beta$. Moreover, $b\bar{b}A$ production is useful for observing the $A \to t\bar{t}$ decay in Type II. The cross section (not shown) ranges from 60–0.2 fb for $m_A \simeq 420$–630 GeV, with only little dependence on $\tan\beta$. The cross section for $gg \to A \to t\bar{t}$ is sizeable (up to 8 pb) for very small $\tan\beta$, but below 0.1 pb for $\tan\beta \gtrsim 2$.

In evaluating the potential for the discovery of A via the $t\bar{t}$ final state, it is noteworthy that $gg \to A \to t\bar{t}$ strongly interferes with the $pp \to t\bar{t}$ SM background, which yields a peak-dip structure in the $t\bar{t}$ invariant mass distribution [64–66]. One should also consider the set of complementary modes, $t\bar{t}A$ associated production in Types I and II, and $b\bar{b}A$ associated production in Type II, followed (in both cases) by $A \to t\bar{t}$, as recently explored in [67–69].[20]

While the sizable cross sections discussed above provide interesting probes of the extended Higgs sector in the alignment limit, the non-standard signatures of $A \to Zh$ and/or $A \to ZH$ shown in Fig. 19 appear to be even more promising.[21] In Type II, there is a strict lower bound on the $gg \to A \to Zh$ cross section, with values above 1 pb at small $\tan\beta$ and at least of order 25 fb at large $\tan\beta$ even at the maximal value of $m_A = 630$ GeV. In Type I, at low $\tan\beta$ the $gg \to A \to Zh$ cross sections fall in the range ~ 1 pb to 20 pb while at large $\tan\beta$ this cross section could be as small as ~ 0.1 fb (or even smaller for $m_A < 220$ GeV). Given that the Run 1 searches in this channel remove a significant portion of the low $\tan\beta$ 2HDM Type I and Type II points, it seems certain that Run 2 results would either be substantially more constraining or reveal a signal.

The cross sections for $gg \to A \to ZH$ are typically at least a factor of 100 smaller than those for the Zh final state. Nevertheless, the $A \to ZH$ decay could provide an additional probe of the small-to-intermediate $\tan\beta$ regime, but will likely be unobservable at large $\tan\beta$ in both Type I and Type II.

---

[20]We thank Ning Chen and Tao Liu for bringing these studies to our attention.
[21]The LHC reach for $gg \to A \to ZH$ and $gg \to A \to Zh$ at $\sqrt{s} = 14$ TeV was previously investigated in [70].
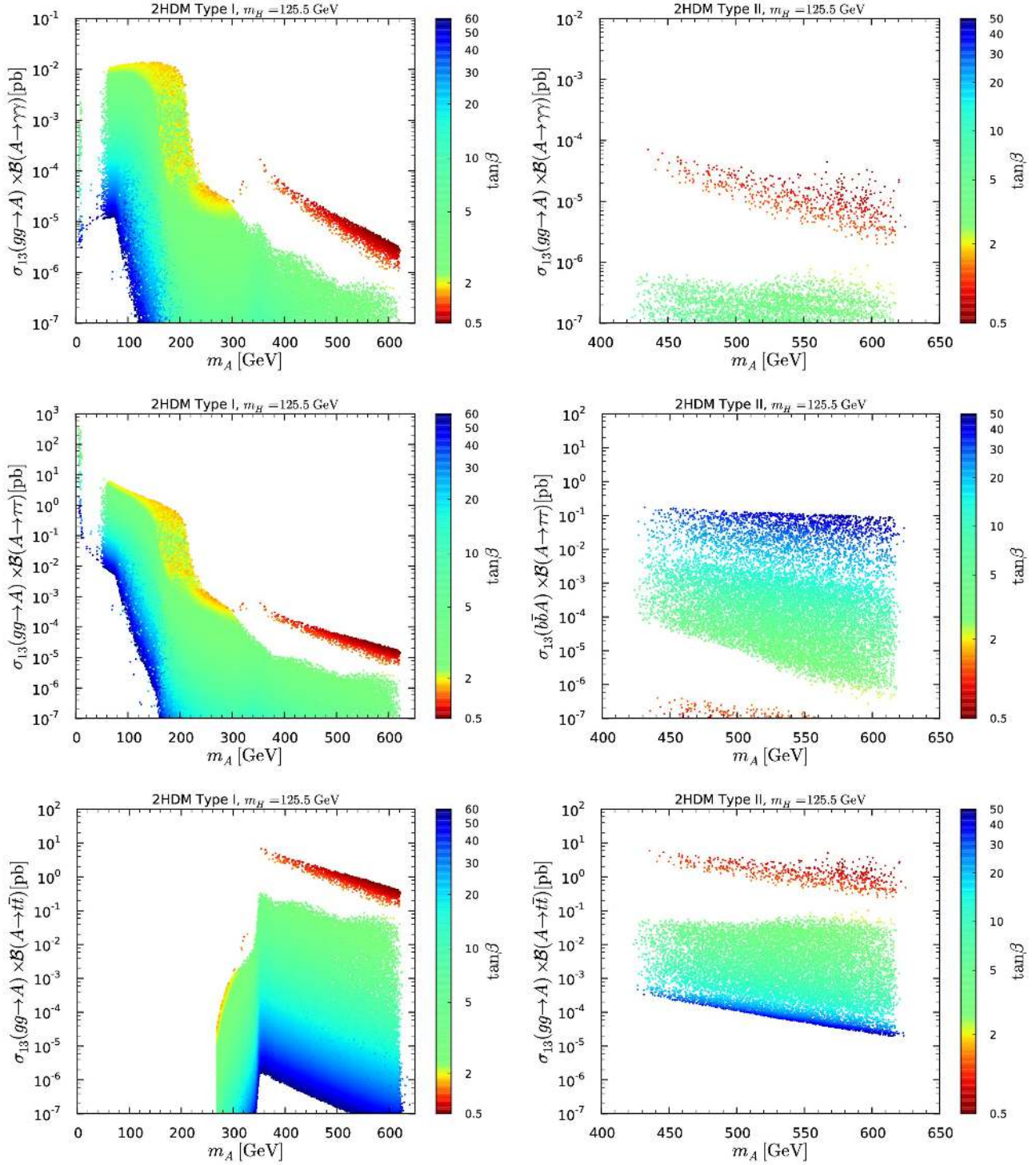
Figure 18: Cross sections times branching ratios in Type I (left) and in Type II (right) for $A \to Y$ signatures at the 13 TeV LHC as functions of m_A with $Y = \gamma\gamma$ (upper panels), $Y = \tau\tau$ (middle panels) and $Y = t\bar{t}$ (lower panels) with $\tan\beta$ color code. Points are ordered from high to low $\tan\beta$.
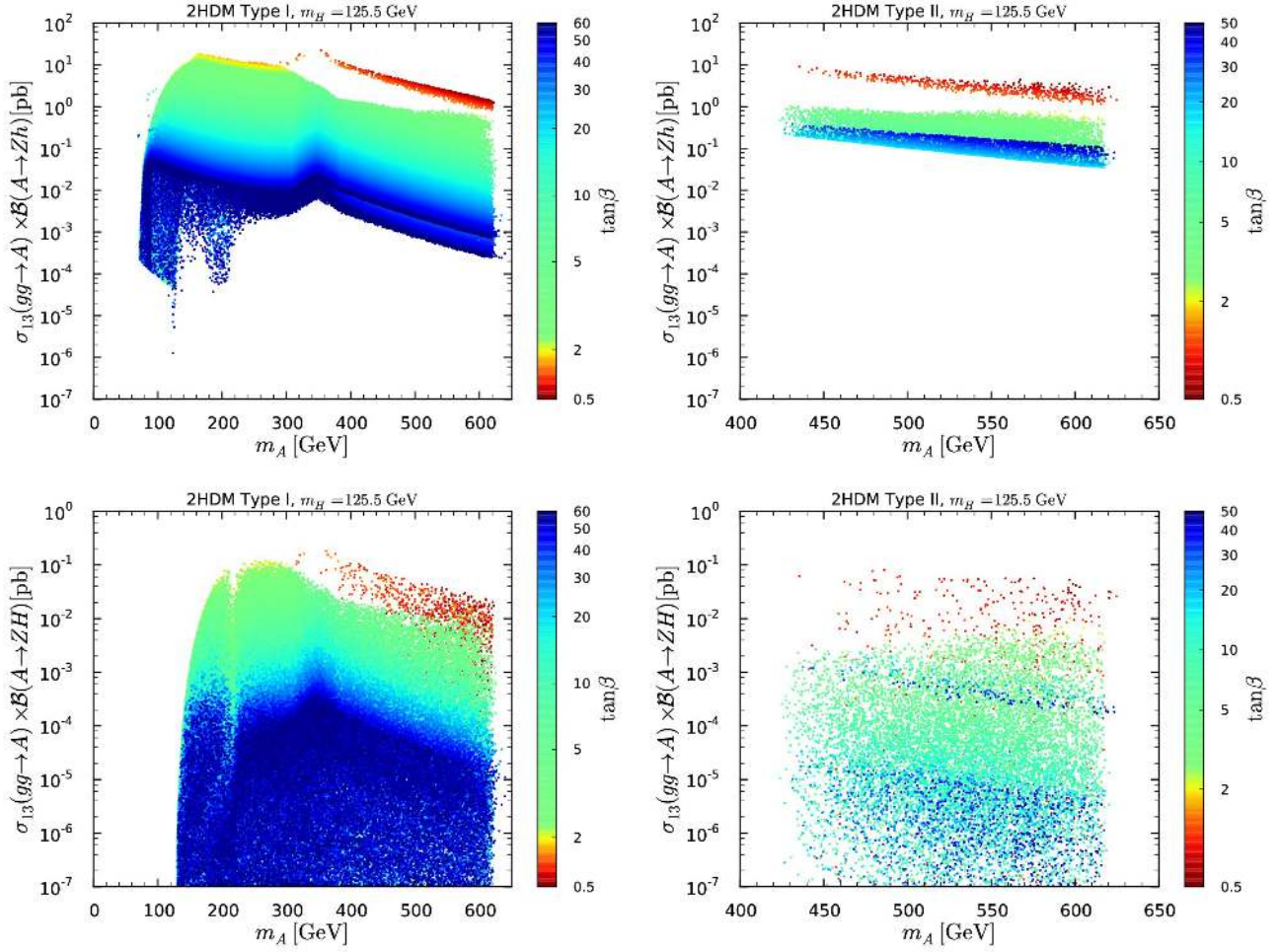
30

Figure 19: Cross sections times branching ratios in Type I (left) and in Type II (right) at the 13 TeV LHC as functions of m_A for $gg \to A \to Zh$ (upper panels) and for $gg \to A \to ZH$ (lower panels) with $\tan\beta$ color code. Points are ordered from low to high $\tan\beta$.

4 Conclusions

In this paper, we studied the approach to the alignment limit of the 2HDM with Type I and Type II Yukawa couplings under the assumption that the observed Higgs boson with mass 125 GeV is the heavier CP-even scalar, H. With the H mass eigenstate being approximately aligned with the direction of the scalar field vacuum expectation value in field space, its coupling to the W and Z bosons tends towards the SM value, $C_V^H \to 1$. Allowing for at most a 1% deviation from unity in C_V^H, we found that deviations in the couplings to fermions of 10–20% are possible while maintaining consistency at 95% CL with the LHC Run 1 Higgs measurements. While C_F^H in Type I and C_U^H in Type II rather quickly approach unity as $|s_{\beta-\alpha}| \to 0$, the approach of the bottom Yukawa coupling to its SM value in the alignment limit is delayed in Type II, with $C_D^H \approx 0.72$–1.12 even for values of $|s_{\beta-\alpha}| \sim 10^{-2}$. Moreover, there can be significant deviations from 1 in the loop-induced coupling to photons: $C_\gamma \approx 0.80$–1.17 (0.88–0.97) in Type I (II). In the case of Type I, the reason for the larger range of C_γ and for its extending also to values above 1 is that the charged Higgs can be light. All these variations in the couplings feed into distinctive behaviors of the signal strengths. Thus, even in the deep alignment regime, where one might naively expect everything to be very SM-like, precise measurements of the signal strengths at 125 GeV can help determine the existence of the extended Higgs sector. Furthermore, correlations between signal strengths are characteristic for the model and can point towards a 2HDM of Type I or Type II.

Comparing with the results from [15], distinguishing $m_h \simeq 125$ GeV from $m_H \simeq 125$ GeV with signal strength measurements and coupling fits alone seems very difficult, unless one finds values that are excluded by $A \to Zh$ in the $m_H \simeq 125$ GeV case. Preferably, and certainly more definitively, one would wish to observe the second CP-even scalar, h. Indeed, in the $m_H \simeq 125$ GeV case studied in this paper, the h must lie below 125 GeV by definition (which also implies that there is no decoupling limit for this type of model). Moreover, for $c_{\beta-\alpha} \geq 0.99$, precision electroweak observables impose an upper limit on the masses of the CP-odd and the charged Higgs of $m_{A,H^\pm} \lesssim 630$ GeV, suggesting that all the extra Higgs states of the 2HDM are at least kinematically accessible at the LHC in this setup. While we did not study the potential for observing the $H^\pm$, direct detection of the h and/or A might be possible in a variety of production $\times$ decay channels. Most exciting and enticing is the channel $gg \to A \to Zh$ which would reveal the presence of both the h and A simultaneously. The associated cross section at $\sqrt{s} = 13$ TeV is at least 20 fb (and can be as large as 10 pb) in Type II. In Type I, $\sigma(gg \to A \to Zh)$ is also large, 10 fb to 30 pb, over most of the parameter space, although for very large $\tan\beta$ it can drop below 1 fb in the ranges $m_A \simeq 90$–250 GeV and $m_A \gtrsim 500$ GeV. The searches for $A \to Zh$ with $Z \to \ell\ell$ and $h \to b\bar{b}$ or $\tau\tau$ are therefore excellent probes for discovering or excluding the 2HDM scenarios with a SM-like H, provided that they are performed *without* requiring a SM-like h with $m_h = 125$ GeV. In fact, CMS has already performed such a search for $A \to Zh$ at $\sqrt{s} = 8$ TeV for general m_A and m_h values (down to 40 GeV), and the limits they obtained are among the most severe constraints for the scenario studied in this paper.

Other channels of high interest include $gg \to h \to \gamma\gamma$ (for $m_h \lesssim 90$ GeV) as well as $gg \to h \to \tau\tau$ (or $\mu\mu$) in Type II. The $\gamma\gamma$ channel may also reveal a light A in Type I if $\tan\beta$ is small. Moreover, $gg \to A \to \tau\tau$ (or $\mu\mu$) can be used to search for a light A in the 10–250 GeV mass range in Type I, while in Type II it would be preferable to exploit the $b\bar{b}A$ production

mode to search for the same A decays (over the relevant mass range of $m_A \simeq 420$–630 GeV). Finally the $t\bar{t}$ final state can be relevant for m_A above 350 GeV in both Type I and Type II if $\tan\beta$ is small.

In short, it is possible that the observed 125 GeV Higgs boson appears SM-like due to the alignment limit of a multi-doublet Higgs sector. However, the alignment limit does not necessarily imply that the additional Higgs states of the model are heavy. Indeed, it is possible that the observed Higgs boson at 125 GeV is the heavier CP-even H, in which case $m_h \in [10, 121.5]$ GeV (since we intentionally avoided the case of h–H mass degeneracy) and $m_{A,H^\pm} < 630$ GeV. Such a scenario, if realized in nature, would lead to exciting new effects to be probed at Run 2 of the LHC.

Acknowledgements

APPENDIX A: Impact of the CMS $A \to Zh$ exclusion

Both ATLAS and CMS have performed searches at $\sqrt{s} = 8$ TeV for a new heavy resonance decaying to a Z boson and a light resonance, with the Z decaying to $\ell\ell = ee$, $\mu\mu$ and the light resonance decaying to $b\bar{b}$ or $\tau\tau$. While the ATLAS analysis [55] required that the light resonance be consistent with the observed 125 GeV Higgs boson, the CMS analysis [17] treated the masses of the two resonances as free parameters and published limits on cross section times branching ratios as functions of the two masses. We can therefore use this CMS result as a constraint on $A \to Zh$ in our study.

For values of $m_A \approx 200$–600 GeV, which is the mass range of particular interest for our analysis, the 95% CL limit on $\sigma(gg \to A \to Zh) \times \mathrm{BR}(Z \to \ell\ell) \times \mathrm{BR}(h \to b\bar{b})$ obtained by CMS is about 100 fb for $m_h \approx 40$–45 GeV, corresponding to the lowest m_h considered in [17]. For heavier m_h, the limit is about 100 fb at $m_A \approx 200$ GeV going down to about 5 fb at $m_A \approx 600$ GeV. As previously mentioned, this is a very severe constraint for the 2HDM in the alignment limit with $m_H \simeq 125$ GeV, cutting out whole slices of parameter space, in particular at low $\tan\beta$. The limit on $\sigma(gg \to A \to Zh) \times \mathrm{BR}(Z \to \ell\ell) \times \mathrm{BR}(h \to \tau\tau)$ has a weaker impact. Indeed, most of the points excluded by the $\ell\ell\tau\tau$ search channel are also excluded by the $\ell\ell b\bar{b}$ channel. Nonetheless, in Type I there is a small corner of parameter space at $\tan\beta \approx 2$
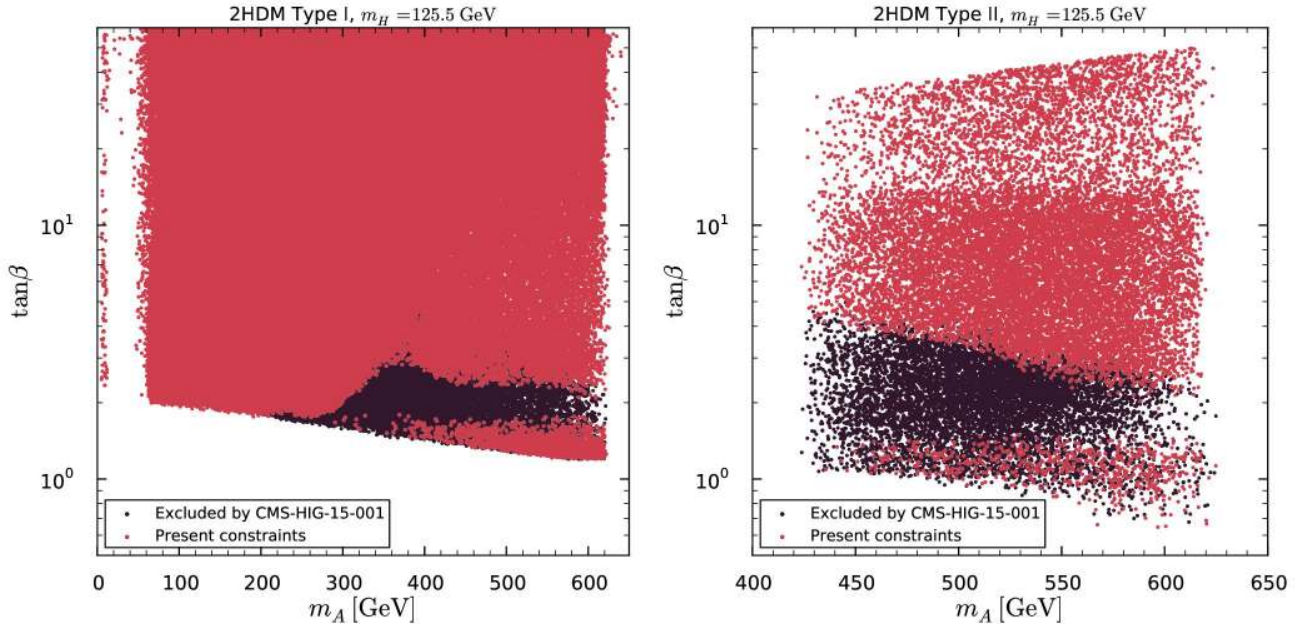
33

Figure 20: Projection of the scan points in the plane $\tan\beta$ vs. m_A, on the left for Type I, on the right for Type II. The red points are consistent with all constraints used in this paper, while the underlying black points are those which are excluded by the CMS $A \to Zh$ ($Z \to \ell\ell$, $h \to b\bar{b}, \tau\tau$) limit [17] after all other constraints have been applied.

and $m_A \lesssim 400$ GeV that is mostly constrained by the $A \to Zh \to \ell\ell\tau\tau$ CMS limit. The impact of the CMS $A \to Zh$ exclusion is illustrated explicitly in Figs. 20–27.

In Fig. 20 we show the projections of the scan points onto the plane $\tan\beta$ versus m_A for both Type I and Type II. The red points are consistent with all constraints used in this paper, while the underlying black points are those which are excluded by the CMS $A \to Zh$ ($Z \to \ell\ell$, $h \to b\bar{b}, \tau\tau$) limits [17] after all other constraints have been applied. We see that the $A \to Zh$ limit from Run 1 excludes a whole slice of parameter space at low $\tan\beta$ and m_A above about 300 GeV. The surviving red points with $m_A > 400$ GeV and $\tan\beta < 2$ have $m_h \lesssim 40$ GeV. Had the CMS analysis been sensitive to light resonance masses below 40 GeV, the entire parameter space with $m_A > 400$ GeV and $\tan\beta \lesssim 2$ would have been ruled out.

The effect on the allowed ranges of the reduced couplings is shown in Figs. 21–24. These plots can be directly compared to the ones in Section 3.2. Particularly striking is the impact on C_γ^H in Type II, where the previously possible deviations below the canonical value of $C_\gamma^H \approx 0.95$ are now largely ruled out. Likewise, large deviations of $C_{HHH} > 1$ are very much restricted by the $A \to Zh$ limit in both Type I and Type II, as shown in Fig. 24. Examples for the impact on the signal strength correlations in Type I and Type II are shown in Fig. 25.

Finally, we examine the impact of the CMS data for $A \to Zh$ on the cross sections for the production of A and h. Significant parts of the parameter space are eliminated, as exemplified in Figs. 26 and 27.
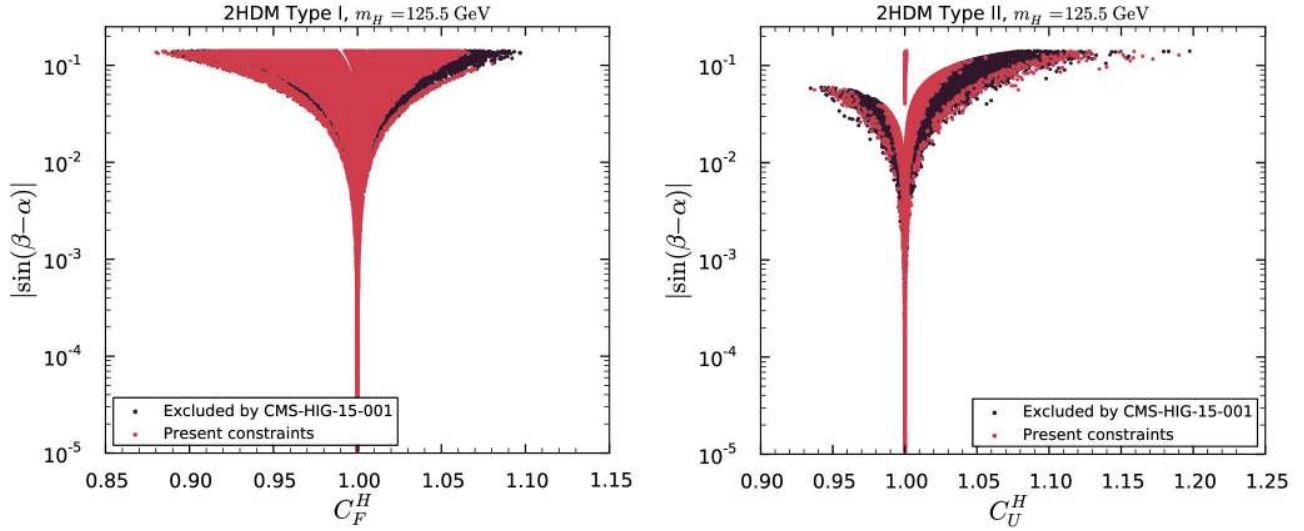
Figure 21: As in Fig. 20 but in the plane $|s_{\beta-\alpha}|$ vs. C_F^H for Type I (left) and $|s_{\beta-\alpha}|$ vs. C_U^H for Type II (right). To be compared to Fig. 3.
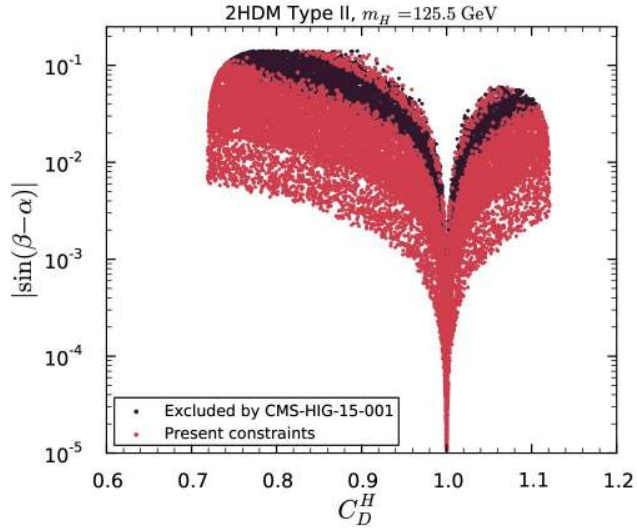

Figure 22: As in Fig. 20 but in the plane $|s_{\beta-\alpha}|$ vs. C_D^H for Type II. To be compared to the left panel of Fig. 4. Note that the figure shows only the positive C_D^H region, the opposite-sign solution not being affected by the CMS $A \to Zh$ constraint.
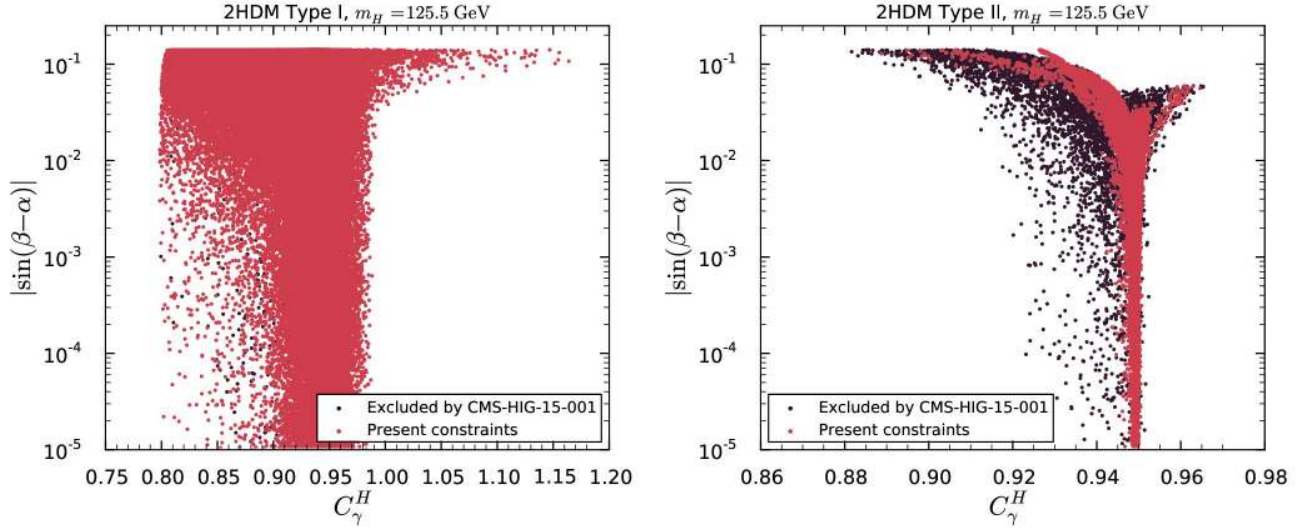
Figure 23: As in Fig. 20 but in the plane $|s_{\beta-\alpha}|$ vs. C_γ^H. To be compared to Fig. 6.
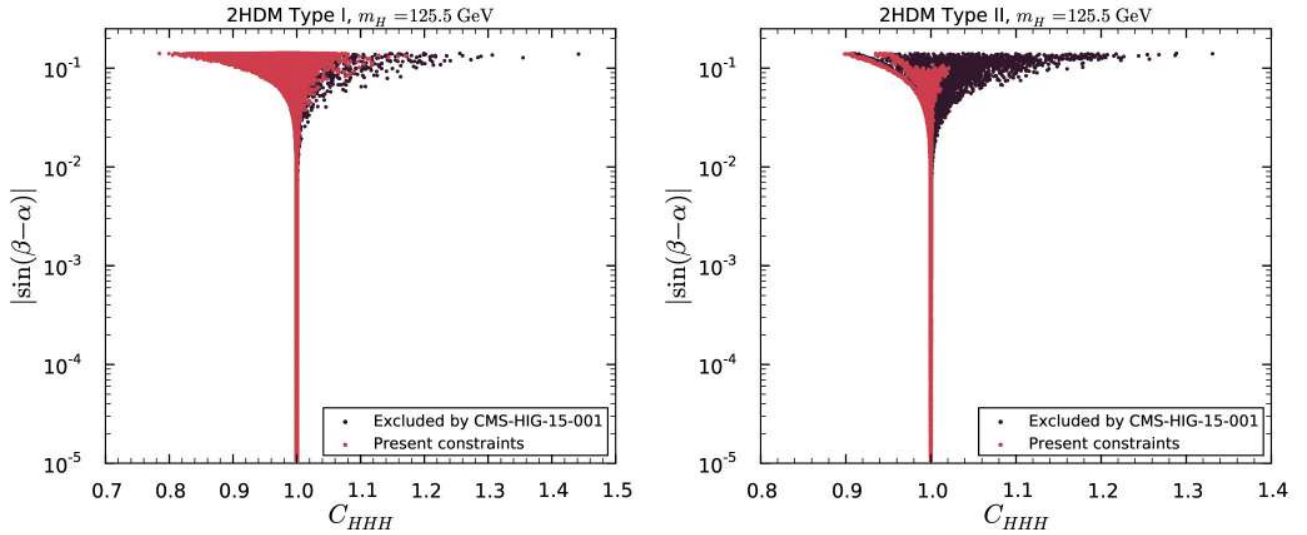

Figure 24: As in Fig. 20 but in the plane $|s_{\beta-\alpha}|$ vs. C_{HHH}. To be compared to Fig. 8.
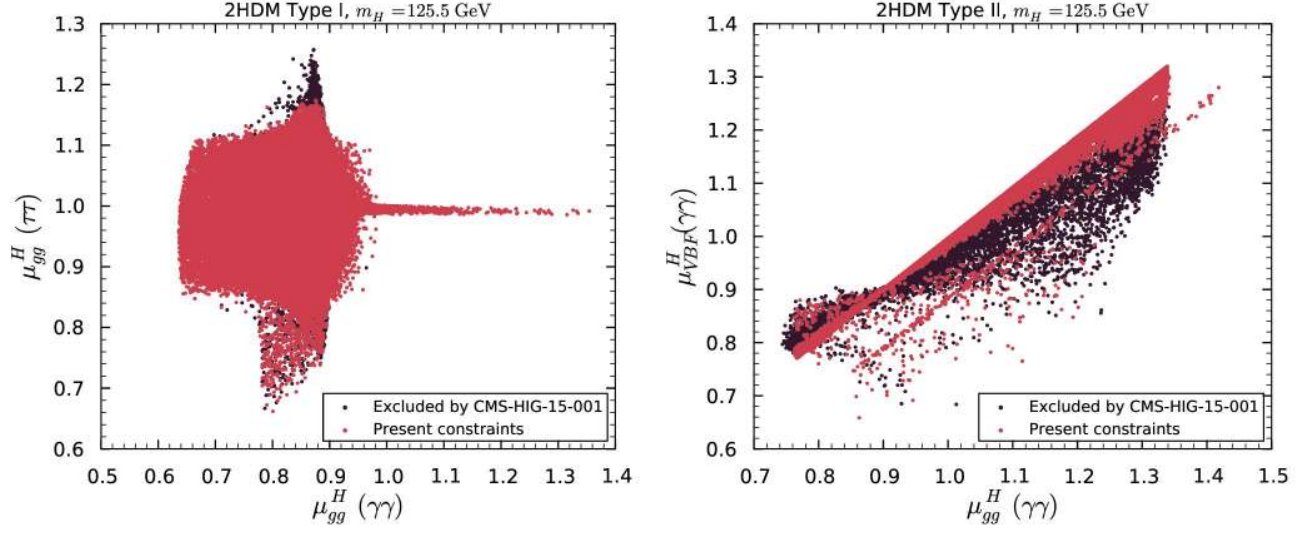
Figure 25: As in Fig. 20 but in the $\mu_{gg}^H(\tau\tau)$ vs. $\mu_{gg}^H(\gamma\gamma)$ in Type I (left panel) and $\mu_{VBF}^H(\gamma\gamma)$ vs. $\mu_{gg}^H(\gamma\gamma)$ in Type II (right panel) planes. To be compared to the fourth and first rows of Fig. 12 and Fig. 13 respectively.
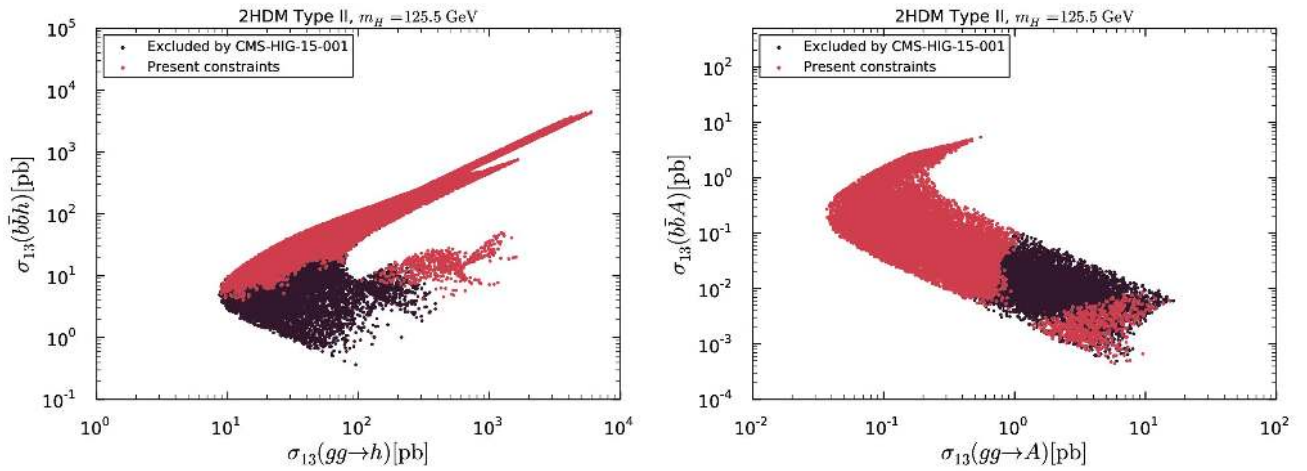

Figure 26: As in Fig. 20, but showing cross sections $\sigma(b\bar{b}X)$ versus $\sigma(gg \to X)$ for $X = h$ (left) and $X = A$ (right) in Type II at the 13 TeV LHC. To be compared to Fig. 15. The effect on the analogous Type I results is very small.
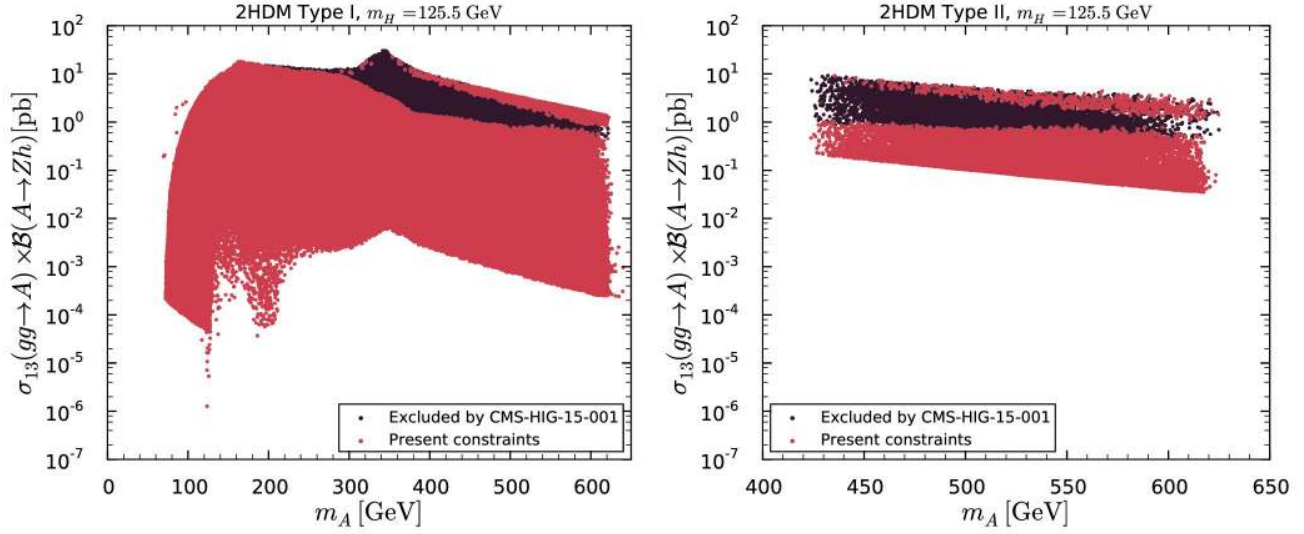
Figure 27: As in Fig. 20, but showing cross section times branching ratio as function of m_A in Type I (left) and in Type II (right) for $gg \to A \to Zh$ at the 13 TeV LHC. To be compared to the upper row of plots of Fig. 19. The strip of red points with $m_A > 400$ GeV and high cross section corresponds to the red points in the bottom-right corners of Fig. 20; the CMS $A \to Zh$ limit is evaded because of a light h, $m_h \lesssim 40$ GeV.

References

[1] **ATLAS** Collaboration, G. Aad et al., *Measurements of the Higgs boson production and decay rates and coupling strengths using pp collision data at $\sqrt{s} = 7$ and 8 TeV in the ATLAS experiment*, `arXiv:1507.04548`.

[2] **CMS** Collaboration, V. Khachatryan et al., *Precise determination of the mass of the Higgs boson and tests of compatibility of its couplings with the standard model predictions using proton collisions at 7 and 8 TeV, Eur. Phys. J.* **C75** (2015) 212, [`arXiv:1412.8662`].

[3] **ATLAS and CMS** Collaboration, *Measurements of the Higgs boson production and decay rates and constraints on its couplings from a combined ATLAS and CMS analysis of the LHC pp collision data at $\sqrt{s} = 7$ and 8 TeV*, Tech. Rep. ATLAS-CONF-2015-044 and CMS-PAS-HIG-15-002, CERN, Geneva, 2015.

[4] J. Bernon, B. Dumont, and S. Kraml, *Status of Higgs couplings after run 1 of the LHC*, *Phys. Rev.* **D90** (2014) 071301, [`arXiv:1409.1588`].

[5] T. Corbett, O. J. P. Eboli, D. Goncalves, J. Gonzalez-Fraile, T. Plehn, and M. Rauch, *The Higgs Legacy of the LHC Run I, JHEP* **08** (2015) 156, [`arXiv:1505.05516`].

[6] J. F. Gunion, H. E. Haber, G. L. Kane, and S. Dawson, *The Higgs Hunter's Guide*. Westview Press, Boulder, CO, 2000.

[7] G. Branco, P. Ferreira, L. Lavoura, M. Rebelo, M. Sher, et al., *Theory and phenomenology of two-Higgs-doublet models*, *Phys. Rept.* **516** (2012) 1–102, [arXiv:1106.0034].

[8] J. F. Gunion and H. E. Haber, *The CP conserving two Higgs doublet model: The Approach to the decoupling limit*, *Phys. Rev.* **D67** (2003) 075019, [hep-ph/0207010].

[9] A. Delgado, G. Nardini, and M. Quiros, *A Light Supersymmetric Higgs Sector Hidden by a Standard Model-like Higgs*, *JHEP* **07** (2013) 054, [arXiv:1303.0800].

[10] N. Craig, J. Galloway, and S. Thomas, *Searching for Signs of the Second Higgs Doublet*, arXiv:1305.2424.

[11] D. M. Asner et al., *ILC Higgs White Paper*, in *Community Summer Study 2013: Snowmass on the Mississippi (CSS2013) Minneapolis, MN, USA, July 29-August 6, 2013*. arXiv:1310.0763.

[12] M. Carena, I. Low, N. R. Shah, and C. E. Wagner, *Impersonating the Standard Model Higgs Boson: Alignment without Decoupling*, *JHEP* **1404** (2014) 015, [arXiv:1310.2248].

[13] H. E. Haber, *The Higgs data and the Decoupling Limit*, arXiv:1401.0152.

[14] P. S. B. Dev and A. Pilaftsis, *Maximally Symmetric Two Higgs Doublet Model with Natural Standard Model Alignment*, *JHEP* **12** (2014) 024, [arXiv:1408.3405].

[15] J. Bernon, J. F. Gunion, H. E. Haber, Y. Jiang, and S. Kraml, *Scrutinizing the alignment limit in two-Higgs-doublet models: $m_h = 125$ GeV*, *Phys. Rev.* **D92** (2015) 075004, [arXiv:1507.00933].

[16] **CMS** Collaboration, V. Khachatryan et al., *Search for a low-mass pseudoscalar Higgs boson produced in association with a b-bbar pair in pp collisions at sqrt(s) = 8 TeV*, arXiv:1511.03610.

[17] **CMS** Collaboration, *Search for H/A decaying into $Z + A/H$, with Z to $\ell\ell$ and A/H to fermion pair*, Tech. Rep. CMS-PAS-HIG-15-001, CERN, Geneva, 2015.

[18] H. E. Haber and O. Stål, *New LHC benchmarks for the $\mathcal{CP}$ -conserving two-Higgs-doublet model*, *Eur. Phys. J.* **C75** (2015) 491, [arXiv:1507.04281].

[19] G. C. Branco, L. Lavoura, and J. P. Silva, *CP Violation*. Oxford University Press, Oxford, UK, 1999.

[20] S. Davidson and H. E. Haber, *Basis-independent methods for the two-Higgs-doublet model*, *Phys. Rev.* **D72** (2005) 035004, [hep-ph/0504050].

[21] H. Huffel and G. Pocsik, *Unitarity Bounds on Higgs Boson Masses in the Weinberg-Salam Model With Two Higgs Doublets*, *Z. Phys.* **C8** (1981) 13.

[22] J. Maalampi, J. Sirkka, and I. Vilja, *Tree level unitarity and triviality bounds for two Higgs models*, *Phys. Lett.* **B265** (1991) 371–376.

[23] S. Kanemura, T. Kubota, and E. Takasugi, *Lee-Quigg-Thacker bounds for Higgs boson masses in a two doublet model*, Phys. Lett. **B313** (1993) 155–160, [`hep-ph/9303263`].

[24] A. G. Akeroyd, A. Arhrib, and E.-M. Naimi, *Note on tree level unitarity in the general two Higgs doublet model*, Phys. Lett. **B490** (2000) 119–124, [`hep-ph/0006035`].

[25] I. F. Ginzburg and I. P. Ivanov, *Tree-level unitarity constraints in the most general 2HDM*, Phys. Rev. **D72** (2005) 115010, [`hep-ph/0508020`].

[26] S. Kanemura and K. Yagyu, *Unitarity bound in the most general two Higgs doublet model*, Phys. Lett. **B751** (2015) 289–296, [`arXiv:1509.06060`].

[27] N. Chakrabarty, U. K. Dey, and B. Mukhopadhyaya, *High-scale validity of a two-Higgs doublet scenario: a study including LHC data*, JHEP **12** (2014) 166, [`arXiv:1407.2145`].

[28] D. Das and I. Saha, *Search for a stable alignment limit in two-Higgs-doublet models*, Phys. Rev. **D91** (2015) 095024, [`arXiv:1503.02135`].

[29] P. Ferreira, H. E. Haber, and E. Santos, *Preserving the validity of the Two-Higgs Doublet Model up to the Planck scale*, Phys. Rev. **D92** (2015) 033003, [`arXiv:1505.04001`].

[30] D. Chowdhury and O. Eberhardt, *Global fits of the two-loop renormalized Two-Higgs Doublet model with soft Z_2 breaking*, JHEP **11** (2015) 052, [`arXiv:1503.08216`].

[31] T. P. Cheng and M. Sher, *Mass Matrix Ansatz and Flavor Nonconservation in Models with Multiple Higgs Doublets*, Phys. Rev. **D35** (1987) 3484.

[32] D. Atwood, L. Reina, and A. Soni, *Phenomenology of two Higgs doublet models with flavor changing neutral currents*, Phys. Rev. **D55** (1997) 3156–3176, [`hep-ph/9609279`].

[33] S. L. Glashow and S. Weinberg, *Natural Conservation Laws for Neutral Currents*, Phys. Rev. **D15** (1977) 1958.

[34] E. Paschos, *Diagonal Neutral Currents*, Phys. Rev. **D15** (1977) 1966.

[35] L. J. Hall and M. B. Wise, *Flavor changing Higgs boson couplings*, Nucl. Phys. **B187** (1981) 397.

[36] V. D. Barger, J. L. Hewett, and R. J. N. Phillips, *New Constraints on the Charged Higgs Sector in Two Higgs Doublet Models*, Phys. Rev. **D41** (1990) 3421–3441.

[37] A. G. Akeroyd, *Nonminimal neutral Higgs bosons at LEP-2*, Phys. Lett. **B377** (1996) 95–101, [`hep-ph/9603445`].

[38] M. Aoki, S. Kanemura, K. Tsumura, and K. Yagyu, *Models of Yukawa interaction in the two Higgs doublet model, and their collider phenomenology*, Phys. Rev. **D80** (2009) 015017, [`arXiv:0902.4665`].

[39] V. Barger, H. E. Logan, and G. Shaughnessy, *Identifying extended Higgs models at the LHC*, Phys. Rev. **D79** (2009) 115018, [`arXiv:0902.0170`].

[40] S. Su and B. Thomas, *The LHC Discovery Potential of a Leptophilic Higgs*, *Phys. Rev.* **D79** (2009) 095014, [arXiv:0903.0667].

[41] N. G. Deshpande and E. Ma, *Pattern of Symmetry Breaking with Two Higgs Doublets*, *Phys. Rev.* **D18** (1978) 2574.

[42] R. Barbieri, L. J. Hall, and V. S. Rychkov, *Improved naturalness with a heavy Higgs: An Alternative road to LHC physics*, *Phys. Rev.* **D74** (2006) 015007, [hep-ph/0603188].

[43] L. Lopez Honorez, E. Nezri, J. F. Oliver, and M. H. G. Tytgat, *The Inert Doublet Model: An Archetype for Dark Matter*, *JCAP* **0702** (2007) 028, [hep-ph/0612275].

[44] A. Goudelis, B. Herrmann, and O. Stl, *Dark matter in the Inert Doublet Model after the discovery of a Higgs-like boson at the LHC*, *JHEP* **09** (2013) 106, [arXiv:1303.3010].

[45] G. Belanger, B. Dumont, A. Goudelis, B. Herrmann, S. Kraml, and D. Sengupta, *Dilepton constraints in the Inert Doublet Model from Run 1 of the LHC*, *Phys. Rev.* **D91** (2015) 115011, [arXiv:1503.07367].

[46] A. Ilnicka, M. Krawczyk, and T. Robens, *The Inert Doublet Model in the light of LHC and astrophysical data – An Update –*, arXiv:1508.01671.

[47] M. Misiak, H. Asatrian, R. Boughezal, M. Czakon, T. Ewerth, et al., *Updated NNLO QCD predictions for the weak radiative B-meson decays*, *Phys. Rev. Lett.* **114** (2015) 221801, [arXiv:1503.01789].

[48] P. Ferreira, J. F. Gunion, H. E. Haber, and R. Santos, *Probing wrong-sign Yukawa couplings at the LHC and a future linear collider*, *Phys. Rev.* **D89** (2014) 115003, [arXiv:1403.4736].

[49] B. Dumont, J. F. Gunion, Y. Jiang, and S. Kraml, *Constraints on and future prospects for Two-Higgs-Doublet Models in light of the LHC Higgs signal*, *Phys. Rev.* **D90** (2014) 035021, [arXiv:1405.3584].

[50] **ATLAS, CMS** Collaboration, G. Aad et al., *Combined Measurement of the Higgs Boson Mass in pp Collisions at $\sqrt{s} = 7$ and 8 TeV with the ATLAS and CMS Experiments*, *Phys. Rev. Lett.* **114** (2015) 191803, [arXiv:1503.07589].

[51] D. Eriksson, J. Rathsman, and O. Stål, *2HDMC: Two-Higgs-Doublet Model Calculator Physics and Manual*, *Comput. Phys. Commun.* **181** (2010) 189–205, [arXiv:0902.0851].

[52] J. Bernon and B. Dumont, *Lilith: a tool for constraining new physics from Higgs measurements*, *Eur. Phys. J.* **C75** (2015) 440, [arXiv:1502.04138].

[53] R. V. Harlander, S. Liebler, and H. Mantler, *SusHi: A program for the calculation of Higgs production in gluon fusion and bottom-quark annihilation in the Standard Model and the MSSM*, *Comput.Phys.Commun.* **184** (2013) 1605–1617, [arXiv:1212.3249].

[54] K. Arnold, M. Bahr, G. Bozzi, F. Campanario, C. Englert, et al., *VBFNLO: A Parton level Monte Carlo for processes with electroweak bosons, Comput. Phys. Commun.* **180** (2009) 1661–1670, [arXiv:0811.4559].

[55] **ATLAS** Collaboration, G. Aad et al., *Search for a CP-odd Higgs boson decaying to Zh in pp collisions at $\sqrt{s} = 8$ TeV with the ATLAS detector, Phys. Lett.* **B744** (2015) 163–183, [arXiv:1502.04478].

[56] J. Bernon, J. F. Gunion, Y. Jiang, and S. Kraml, *Light Higgs bosons in Two-Higgs-Doublet Models, Phys. Rev.* **D91** (2015) 075019, [arXiv:1412.3385].

[57] J. F. Gunion and X.-G. He, *Determining the CP nature of a neutral Higgs boson at the LHC, Phys. Rev. Lett.* **76** (1996) 4468–4471, [hep-ph/9602226].

[58] **ATLAS** Collaboration, G. Aad et al., *Search for neutral Higgs bosons of the minimal supersymmetric standard model in pp collisions at $\sqrt{s} = 8$ TeV with the ATLAS detector, JHEP* **1411** (2014) 056, [arXiv:1409.6064].

[59] **CMS** Collaboration, V. Khachatryan et al., *Search for neutral MSSM Higgs bosons decaying to a pair of tau leptons in pp collisions, JHEP* **1410** (2014) 160, [arXiv:1408.3316].

[60] M. E. Peskin and T. Takeuchi, *Estimation of oblique electroweak corrections, Phys. Rev.* **D46** (1992) 381–409.

[61] F. Mahmoudi and O. Stal, *Flavor constraints on the two-Higgs-doublet model with general Yukawa couplings, Phys. Rev.* **D81** (2010) 035016, [arXiv:0907.1791].

[62] M. E. Peskin, *Estimation of LHC and ILC Capabilities for Precision Higgs Boson Coupling Measurements*, in *Community Summer Study 2013: Snowmass on the Mississippi (CSS2013) Minneapolis, MN, USA, July 29-August 6, 2013*, 2013. arXiv:1312.4974.

[63] **CMS** Collaboration, *Search for new resonances in the diphoton final state in the mass range between 80 and 115 GeV in pp collisions at $\sqrt{s} = 8$ TeV*, Tech. Rep. CMS-PAS-HIG-14-037, CERN, Geneva, 2015.

[64] D. Dicus, A. Stange, and S. Willenbrock, *Higgs decay to top quarks at hadron colliders, Phys. Lett.* **B333** (1994) 126–131, [hep-ph/9404359].

[65] R. Frederix and F. Maltoni, *Top pair invariant mass distribution: A Window on new physics, JHEP* **01** (2009) 047, [arXiv:0712.2355].

[66] S. Jung, J. Song, and Y. W. Yoon, *Dip or nothingness of a Higgs resonance from the interference with a complex phase, Phys. Rev.* **D92** (2015) 055009, [arXiv:1505.00291].

[67] N. Craig, F. D'Eramo, P. Draper, S. Thomas, and H. Zhang, *The Hunt for the Rest of the Higgs Bosons, JHEP* **06** (2015) 137, [arXiv:1504.04630].

[68] J. Hajer, Y.-Y. Li, T. Liu, and J. F. H. Shiu, *Heavy Higgs Bosons at 14 TeV and 100 TeV*, *JHEP* **11** (2015) 124, [arXiv:1504.07617].

[69] N. Chen, J. Li, and Y. Liu, *LHC searches for heavy neutral Higgs bosons with a top jet substructure analysis*, arXiv:1509.03848.

[70] B. Coleppa, F. Kling, and S. Su, *Exotic Decays Of A Heavy Neutral Higgs Through HZ/AZ Channel*, *JHEP* **09** (2014) 161, [arXiv:1404.1922].